EUROPEAN COMMISSION

Community research

GOBIERNO DE ESPAÑA | MINISTERIO DE ECONOMÍA Y COMPETITIVIDAD | Ciemat Centro de Investigaciones Energéticas, Medioambientales y Tecnológicas

PEBS Long-term Performance of Engineered Barrier Systems

Long-term Performance of Engineered Barrier Systems PEBS

EB experiment
Laboratory post-mortem analyses report

(DELIVERABLE-N°: D2.1-7)

Contract (grant agreement) number: FP7 249681

CIEMAT Technical Report CIEMAT/DMA/2G210/01/2014

Author(s): M.V. Villar, R. Campos, L. Gutiérrez-Nebot

Reporting period:
Date of issue of this report: January 10th 2014

Start date of project: 01/03/10 Duration : 48 Months

Project co-funded by the European Commission under the Seventh Euratom Framework Programme for Nuclear Research &Training Activities (2007-2011)		
Dissemination Level		
PU	Public	**PU**
RE	Restricted to a group specified by the partners of the [acronym] project	
CO	Confidential, only for partners of the [acronym] project	

EURATOM

Contents

1 Introduction: the EB experiment

The EB experiment was run by ENRESA at the Mont Terri Underground Research Laboratory in Switzerland, starting in October 2000, with the aim of demonstrating that automated production of a Granular Bentonite Material (GBM) and its emplacement in the upper part of a clay barrier were feasible (ENRESA 2005). The lower part of the barrier was composed by blocks of compacted bentonite on which the dummy canister rested. The EB niche excavated in the Opalinus clay was 15 m long and had a geometry of a horseshoe section, 2.55 m high and 3 m wide (Figure 1).

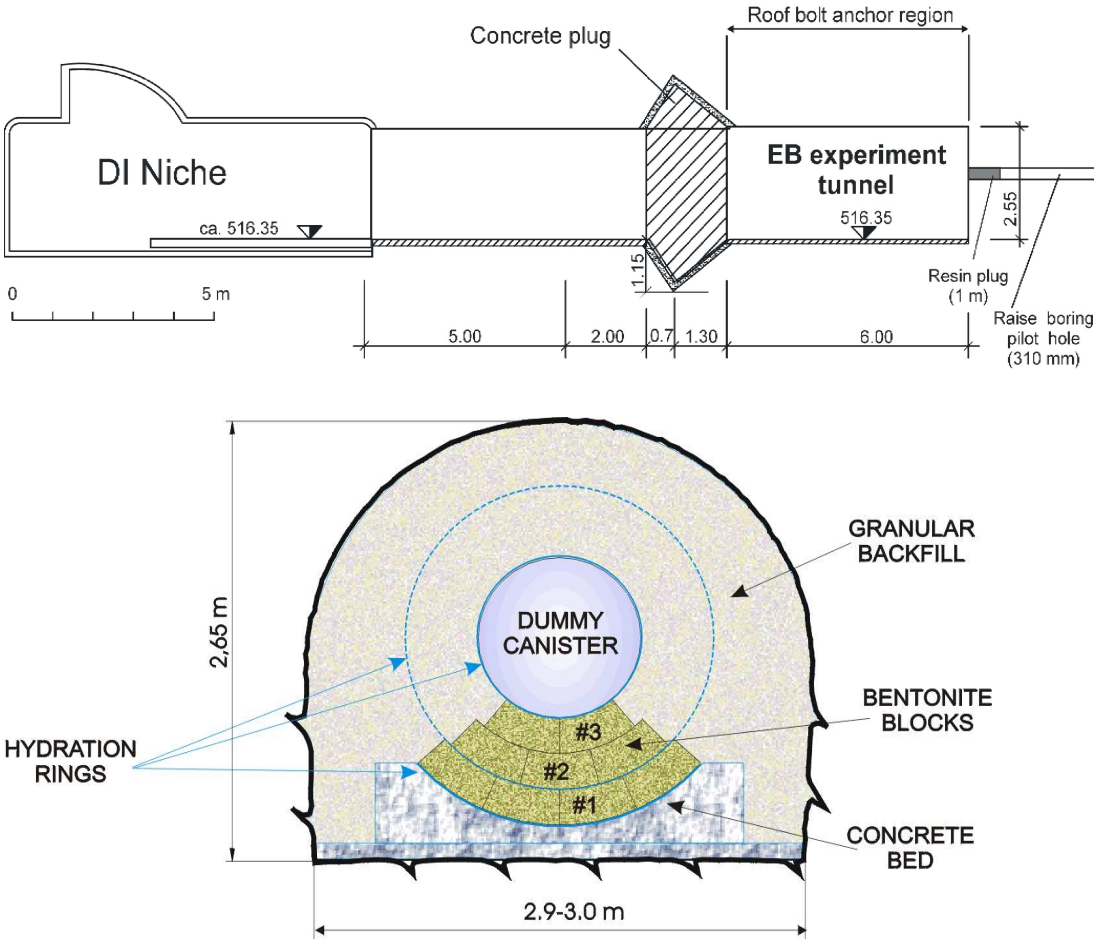

Figure 1: EB niche at Mont Terri URL, longitudinal and cross sections (ENRESA 2005)

According to the measurements performed during installation, in the EB test section an average dry density of 1.36 g/cm^3 of the emplaced GBM was obtained, although some segregation during the emplacement and density inhomogeneities were acknowledged. According to the laboratory characterization of the GBM (ENRESA 2005), for this dry density value it was estimated that the hydraulic conductivity was lower than $5 \cdot 10^{-12}$ m/s and the swelling pressure about 1.3 MPa. The artificial hydration of the buffer material started on May 2002 through a series of porous tubes that crossed along the GBM and the bentonite blocks as shown in Figure 2. To enhance the water homogeneous distribution, the concrete bed, the surface of the container and the three rings of the bentonite blocks bed were covered with geotextile. Hydration was carried out with Pearson water coming from a deposit. The Pearson water is a predominantly sodium-chloride solution of 19 g/L salinity and has a composition similar to the

Opalinus Clay formation pore water. It has a density of 1.020 g/cm^3 (Pearson 1998) and its chemical composition is indicated in Table I.

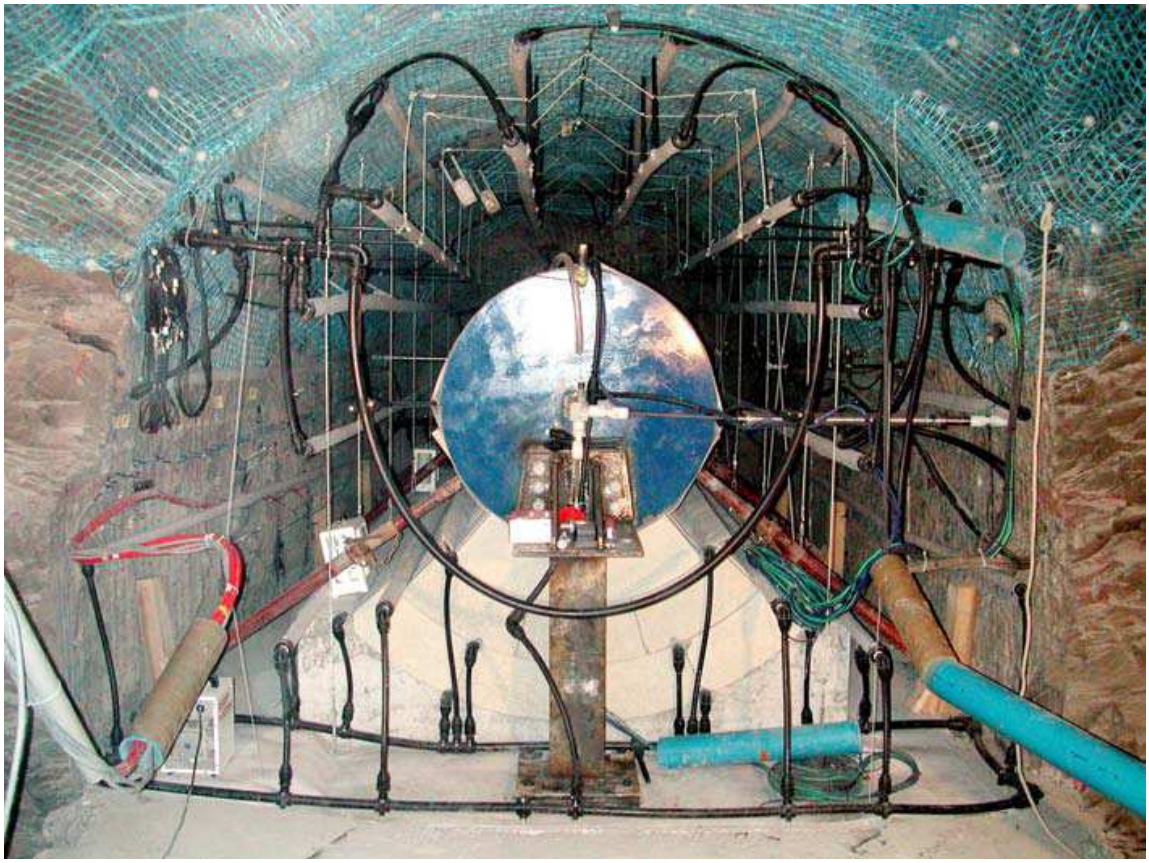

Figure 2: Appearance of the concrete and bentonite blocks bed, dummy canister and hydration system before the installation of the GBM (ENRESA 2005)

Table I: Chemical composition of Pearson water (mg/L)

Cl^-	SO_4^{2-}	HCO_3^-	Mg^{2+}	Ca^{2+}	Na^+	K^+	Sr^+	pH
10635.90	1354.41	25.75	413.19	1034.06	5550.01	62.95	44.69	7.6

2 Dismantling and sampling

The test run under isothermal conditions (average temperature 16°C) for 10.5 years. The dismantling of the test started on October 2012 with the demolition of the concrete plug, which took almost a month, and went on until February 2013. Figure 3 shows the appearance of the GBM and the bentonite blocks as the test was dismantled, as well as details of the GBM-block contact. The GBM looked completely homogeneous and every void in the barrier had been filled. The contact between the blocks and the GBM was easily recognisable, since the blocks presented a coarse-grained texture, whereas no grains could be identified in the GBM. The pictures show also the numerous tubes and cables that crossed the barrier and the blocks, the appearance of the steel container, the concrete bed and the geotextile layers that separated the three rings of blocks.

Figure 3: Appearance of the GBM (left up), the bentonite blocks (right up), and the GBM-blocks contact (bottom) upon dismantling.

The dimensions of the blocks were measured both on site and in the laboratory, and their increase confirms that they swelled during the test and also after dismantling, when the pressures were released. The blocks closer to the concrete plug swelled mainly in the longitudinal direction, whereas in the rest of sections the change in blocks' vertical dimensions indicates the uplift of the canister (Palacios et al. 2013, Villar 2013).

Samples of the GBM, the bentonite blocks, the concrete bed and the concrete plug, the Opalinus clay, and other materials were taken for analysis in the laboratory. Additionally, dry density and water content determinations of the bentonite were performed on site by the AITEMIN team (Palacios et al. 2013). These determinations were also performed at CIEMAT in bentonite samples that were quickly packed after being taken and sent to CIEMAT laboratories. The packing consisted of a plastic film and two aluminium foil bags that were vacuumed before being sealed.

The bentonite samples analysed at CIEMAT laboratories belong to the sampling sections A1-25, CMT1, CMT2, E, B2 and CMT3 (Figure 5). The samples were taken following approximately radii, as shown in Figure 4. Initially only the sections CMT1, CMT2 and CMT3 were to be sampled for CIEMAT (AITEMIN 2012), but once the dismantling started it was decided to take samples from the other sections in order to crosscheck the water content and dry density values obtained on site. Samples from the GBM were referenced starting by "B-S", followed by the section name and then a correlative number. The blocks were given references starting by "B-B" and in the laboratory they were subsampled in three different levels: up (a), middle (m) and bottom (h), according to the position of the block in the barrier.

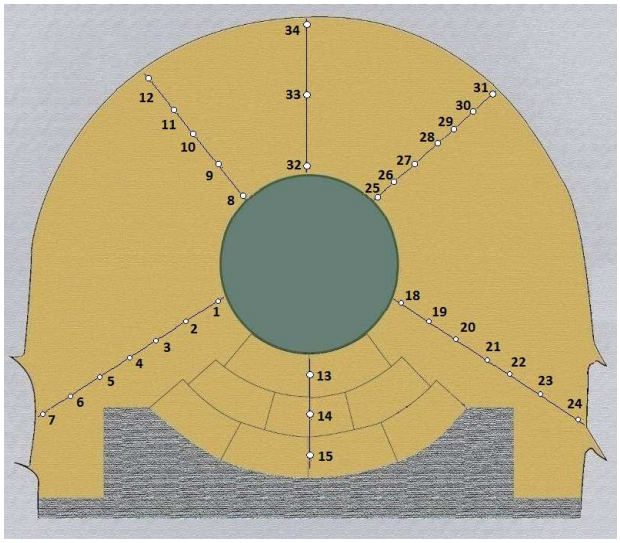

A1-25

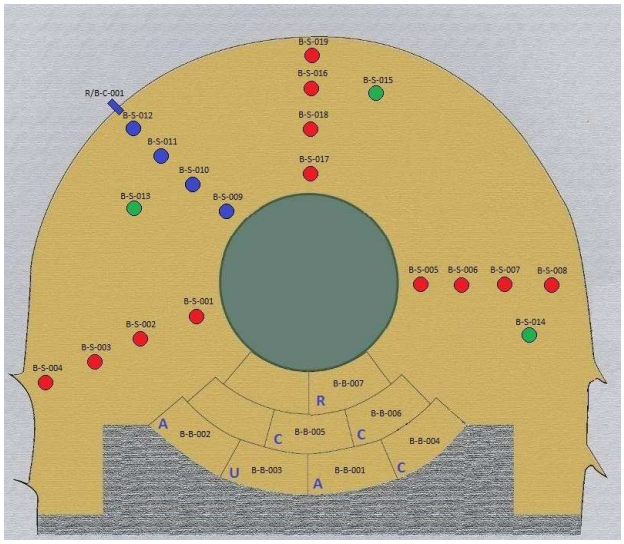

CMT1

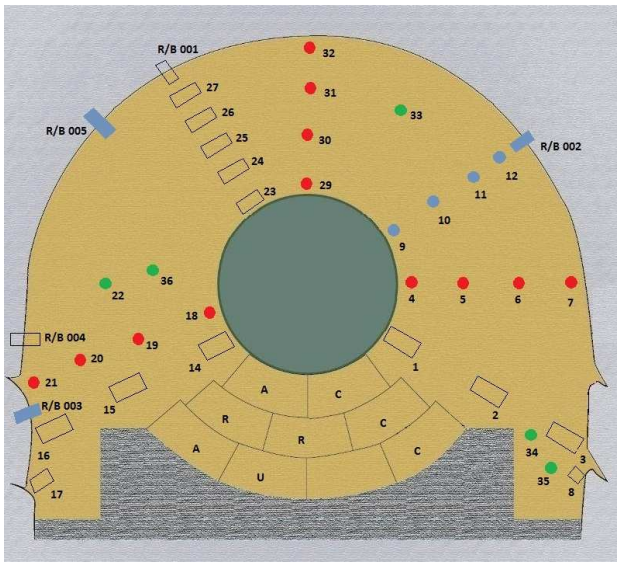

CMT2

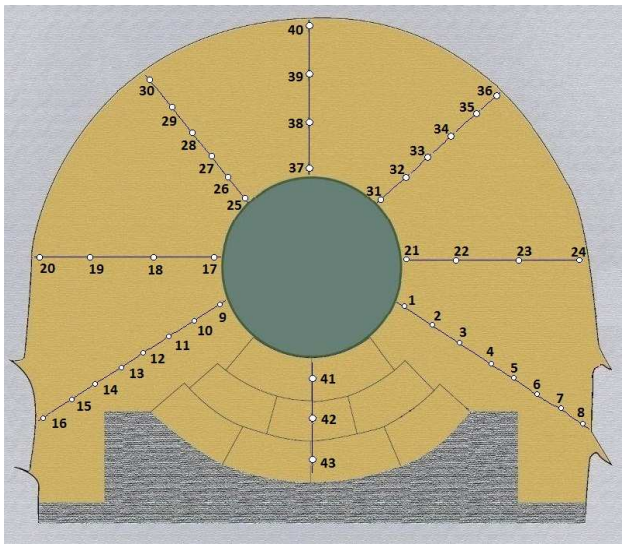

E

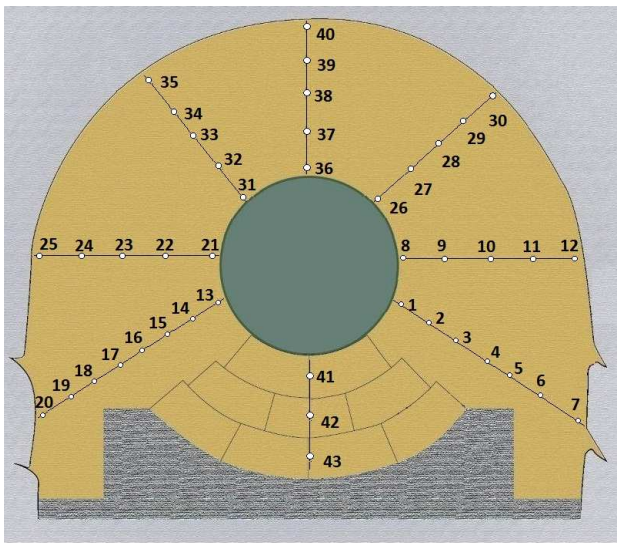

B2

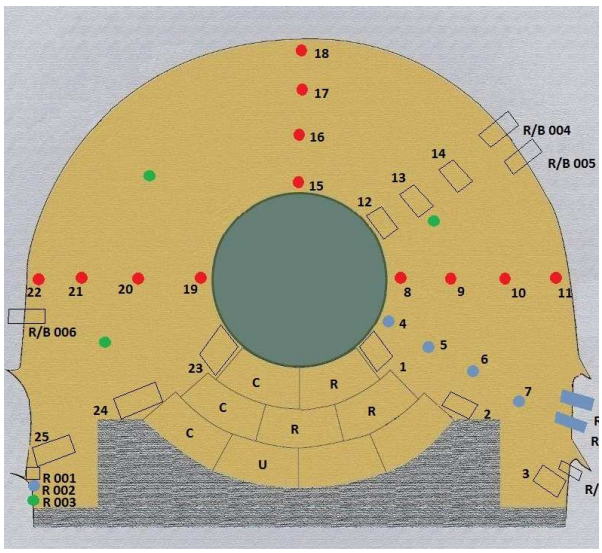

CMT3

Figure 4: Cross section of the sampling sections showing the location of the bentonite samples (in sections CMT1, CMT2 and CMT3 the GBM samples sent to CIEMAT are indicated with red circles or rectangles and the blocks with a C) (AITEMIN 2012)

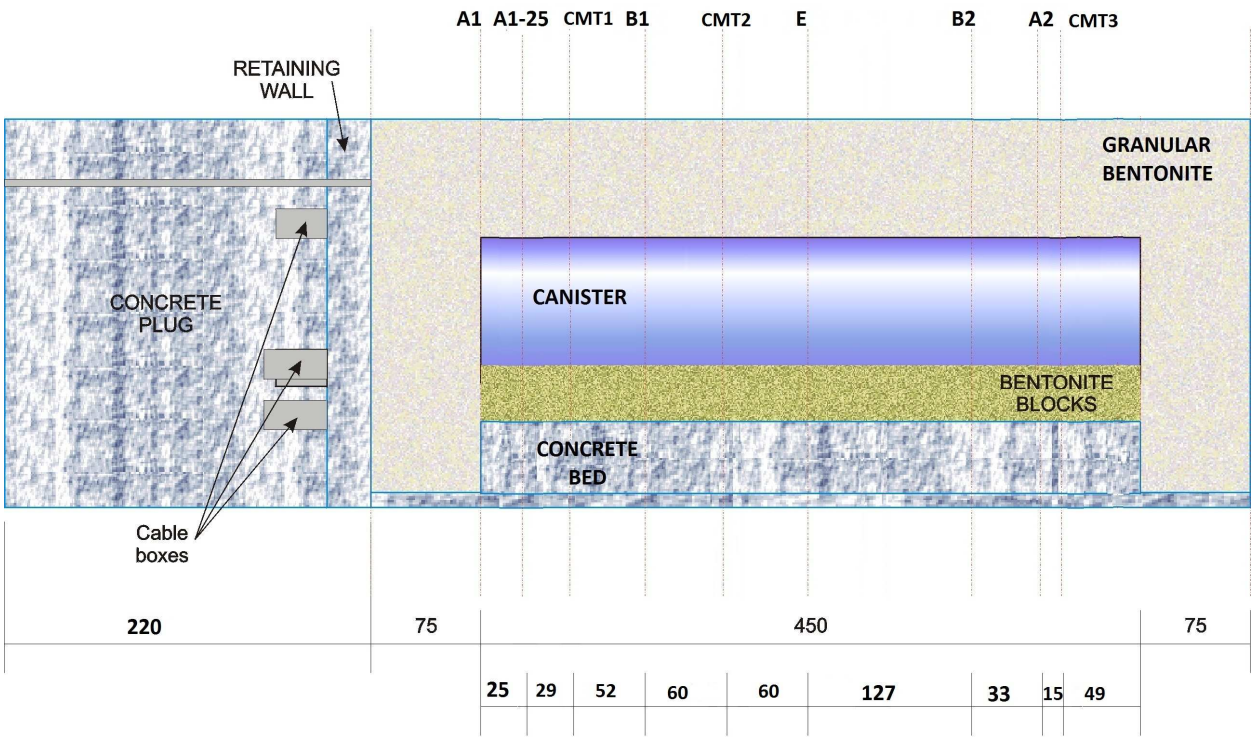

Figure 5: Longitudinal cross-section of the EB test at Mont Terri and bentonite sampling sections (distances in cm, AITEMIN 2012)

This report summarises first the results obtained concerning the physical state of the samples (namely dry density and water content), which was described in Villar (2013) and then details the additional analyses performed at CIEMAT concerning the thermo-hydro-mechanical characterisation of the bentonite, including permeability, thermal conductivity and swelling capacity.

3 Material

The GBM used in the EB experiment was prepared from FEBEX bentonite dried and milled in a three-step process to produce a fine grade powder with a water content of 3.3%. Later, a commercial plant with an in-line highly automated briquetting process produced coarse (>7 mm) and fine (0.4-2 mm) grained materials with dry densities of 2.11 and 2.13 g/cm^3, respectively. These two grain size fractions were subsequently combined after several trials to produce a material with a granulometric Simonis curve, which was used for the *in situ* emplacement (ENRESA 2005). On the other hand, the blocks used came from the series that was manufactured for the FEBEX *in situ* test in 1997, and had a dry density of 1.69 g/cm^3 and a water content of 14.4%.

The physico-chemical properties of the FEBEX bentonite, as well as its most relevant thermo-hydro-mechanical and geochemical characteristics obtained during the projects FEBEX I and II were summarised in the final report of the project (Villar 2002, ENRESA 2006). The FEBEX bentonite was extracted from the Cortijo de Archidona deposit (Almería, Spain). The processing at the factory consisted of disaggregation and gently grinding, drying at 60°C and sieving by 5 mm, and this was the material used for the laboratory characterisation, the FEBEX blocks manufacturing and the GBM preparation.

The montmorillonite content of the FEBEX bentonite is above 90 wt.%. The smectitic phases are actually made up of a smectite-illite mixed layer, with 10-15 wt.% of illite layers. Besides, the bentonite contains variable quantities of quartz, plagioclase, K-felspar, calcite, and cristobalite-trydimite. The liquid limit of the bentonite is 102±4%, the plastic limit 53±3%, the specific gravity 2.70±0.04, and 67±3 percent of particles are smaller than 2 μm. The hygroscopic water content is 13.7±1.3 percent. The total specific surface area obtained using the Keeling hygroscopicity method is 725 m^2/g. The cation exchange capacity is 102±4 meq/100g, the main exchangeable cations being calcium, magnesium and sodium. The predominant soluble ions are chloride, sulphate, bicarbonate and sodium.

The saturated hydraulic conductivity to deionised water (k_w, m/s) of samples of untreated FEBEX bentonite compacted at different dry densities is exponentially related to dry density (ρ_d, g/cm^3) for dry densities of less than 1.47 g/cm^3, according to the following relation:

$$\log k_w = -6.00\ \rho_d - 4.09 \quad [1]$$

The determinations were done at room temperature. The variation in the experimental values with respect to these fittings is smaller for low densities than it is for higher values, with an average –in absolute values– of 30 percent.

The swelling pressure (P_s, MPa) of FEBEX samples compacted with their hygroscopic water content and flooded with deionised water up to saturation at room temperature and constant volume conditions can be related to dry density (ρ_d, g/cm^3) through the following Equation:

$$\ln P_s = 6.77\ \rho_d - 9.07 \quad [2]$$

In this case, the difference between experimental values and this fitting is, on average, 25 percent.

Numerous swelling deformation tests performed in oedometers allowed determining an empirical relation between swelling strain (ε, %), initial dry density (ρ_{d0}, g/cm^3), initial water content (w_0, %) and vertical pressure (σ, MPa) (Villar & Lloret 2008):

$$\varepsilon = [(-12.12 \ln \rho_{d0} + 1.89) \ln \sigma + (36.81\ \rho_{d0} - 53.59)] \ln w_0 + (38.27 \ln \rho_{d0} - 1.25) \ln \sigma + (-149.05\ \rho_{d0} + 211.42) \quad [3]$$

The retention curve of the bentonite was determined in samples compacted to different dry densities at different temperatures. The volume of the samples remained constant during the determinations, since they were confined in constant volume cells. Fitting the data from these laboratory determinations, the empirical Equation 4 can be obtained (Villar et al. 2012b):

$$w = \left(\left(b \cdot n^c \cdot e^{-\alpha (T - T_0)} \right) \cdot \left[1 + \left(\frac{s}{P_0 \cdot e^{-\eta (n - n_0)} \cdot e^{-\alpha (T - T_0)}} \right)^{\frac{1}{1-\lambda_1}} \right]^{-\lambda_1} \right) \cdot \left(1 - \left(\frac{s}{P_{sec}} \right)^{\lambda_2} \right) \cdot \left(S_r - S_{lr} \right) \quad [4]$$

where w is the water content in percentage, n and n_0 the porosity and reference porosity, s the suction in MPa, T and T_0 the temperature and reference temperature in °C, S_r and S_{lr} the liquid degree of saturation and liquid residual degree of saturation, P_0, P_{sec}, λ_1 and λ_2 parameters to define the retention curve at reference temperature and porosity, and b, c, α and η fitting parameters to take into account the influence of temperature and porosity. The values of parameters are indicated in Table II. The differences between measured values and the estimated values using Equation 4 are smaller than 2% in terms of water content.

Table II: Values of parameters in Equation 4

b	c	P_0 (MPa)	λ_1	λ_2	η	n_0	α (1/°C)	T_0 (°C)	P_{sec} (MPa)	S_{lm}	S_{lr}
145	1.9	25	0.2	1.1	20	0.4	0.0015	20	1000	1.0	0.01

The thermal conductivity (λ, W/m·K) of the compacted bentonite at laboratory temperature is related to the degree of saturation (S_r) through the following expression:

$$\lambda = \frac{0.57 - 1.28}{1 + \exp^{(S_r - 0.65)/0.100}} + 1.28 \quad [5]$$

Although this characterisation was performed in granular material with a grain size <5 mm, it was proved that the saturated hydro-mechanical properties of pellets mixtures are similar to those of granulates (Imbert & Villar 2006).

4 Methodology of laboratory tests

Until their analysis, the samples sent from Mont Terri were kept at CIEMAT facilities in a storage room in which the temperature was between 7 and 16°C and the relative humidity between 70 and 90%. The samples were taken one at a time out of the storage room and unpacked in the laboratory. The size and condition of the samples was very variable. Most of the blocks kept their original shape, but some of them came in pieces (Figure 6). Overall, the samples from the GBM looked homogeneous, but occasionally they presented blue spots or areas of different grain size (Figure 7). Samples from the GBM had references starting by "B-S", followed by the section name and then a correlative number. The blocks had references starting by "B-B" and in the laboratory they were subsampled in three different levels: up (a), middle (m) and bottom (h), according to the position of the block in the barrier.

The dry density and water content were determined in small samples to complement the determinations performed on site. Mercury intrusion porosimetry tests and measurement of the basal spacing of the smectite were also done in most of the subsamples. Suction and thermal conductivity measurements were performed in intact samples of the appropriate size and shape. In addition, samples were specifically prepared to determine hydraulic conductivity and swelling capacity following the procedures described below.

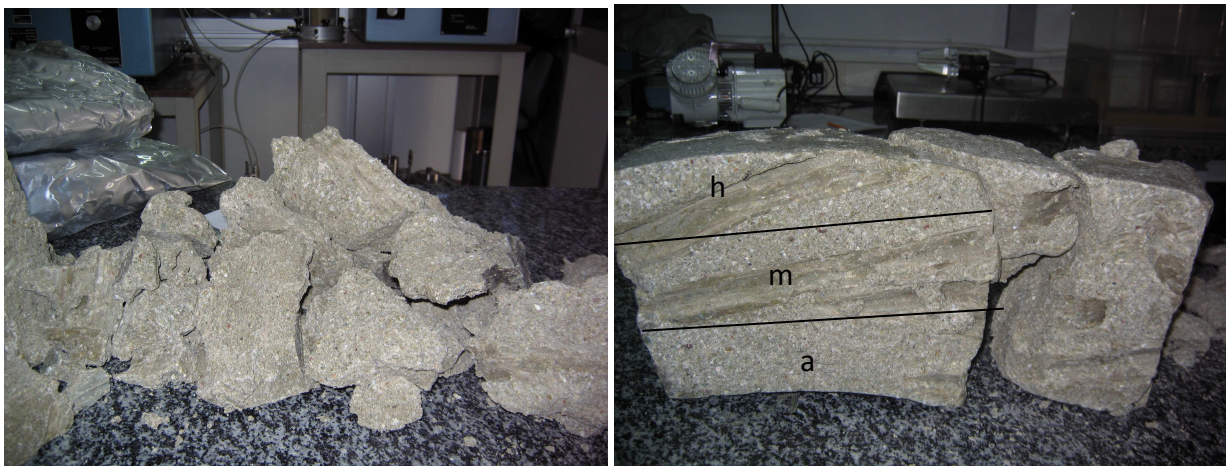

Figure 6: Appearance of blocks after unpacking and definition of subsampling sections

Figure 7: Appearance of some GBM samples

4.1 DRY DENSITY AND WATER CONTENT

The samples for the water content and dry density determinations were prepared by trimming regular specimens of the right size, with volumes of between 6 and 13 cm^3. Two specimens were trimmed and analysed from each GBM sample. The subsamples from the blocks were taken at three different distances from the container (up, middle, down), and for each distance at least two specimens were used. The process of trimming took some minutes, and during this time some drying of the sample could have taken place, because the samples remained exposed to drier room conditions than those in the barrier. This was evaluated and it was concluded that the decrease in water content during laboratory manipulation would be between 0.7 and 1.5%, which could imply a decrease in the degrees of saturation obtained of 2% in the worst cases (Villar 2013).

The gravimetric water content (w) is defined as the ratio between the weight of water and the weight of dry solid expressed as a percentage. The weight of water was determined as the difference between the weight of the sample and its weight after oven drying at 110°C for 48 h (weight of solid). Dry density (ρ_d) is defined as the ratio between the weight of the dry sample and the volume occupied by it prior to drying. The volume of the specimens was determined by immersing them in a recipient containing mercury and by weighing the mercury displaced, as established in UNE Standard 7045 "Determination of soil porosity". The same samples whose volumes had been determined were used for the water content determination. Additionally, in some cases larger samples were used just for water content determination.

4.2 SUCTION MEASUREMENT

In some samples of size large enough the relative humidity and temperature were measured using either a capacitive sensor or a psychrometer (Figure 8, Figure 9). Since the degree of saturation of the samples was very high, the measurement range of the capacitive sensors was not suitable, because their accuracy for relative humidities between 90 and 100% is 2%. Consequently, it was decided to use exclusively psychrometers. In both cases the sensors were inserted in holes drilled in the bentonite and sealed with the bentonite itself. The samples were kept wrapped in plastic films or in bags to avoid water content lost during the measurements. The equilibration time for the capacitive sensors was less than 2 hours and for the psychrometers of at least 24 hours. The suction in the pores of the sample (s, in MPa) is related to the relative humidity (RH, %) and the temperature (T, absolute temperature) measured by the sensors by means of Kelvin's law:

$$s = -10^{-6}\frac{R \times T}{V_w}\ln\left(\frac{\mathrm{HR}}{100}\right) \qquad [6]$$

where R is the universal constant of the gases (8.3143 J/mol·K) and V_w is the molar volume of the water ($1.80 \cdot 10^{-5}$ m^3/mol).

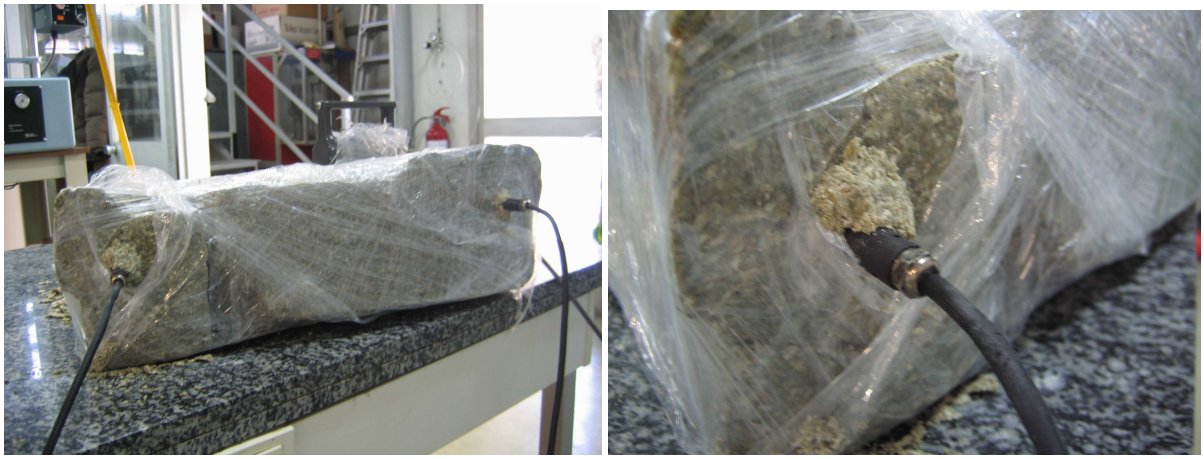

Figure 8: Insertion of capacitive sensors in blocks for measurement of RH and *T*

Figure 9: Measurement of relative humidity and temperature with psychrometers

4.3 PORE SIZE DISTRIBUTION

The pore size distribution was determined by mercury intrusion porosimetry (MIP) in subsamples of GBM and blocks of sizes lower than 3 cm^3. This technique allows the determination of pore size distribution by injecting mercury into the sample at different pressures while controlling the volume intruded. The pressure applied can be related to the minimum pore diameter intruded, taking into account the characteristics of the fluid. The ratio of the volume of mercury intruded (pore volume) to applied pressure (which conditions the minimum pore diameter) allows distribution curves to be obtained establishing the percentage of pores of a size included within a given range.

The samples were put in the ice condenser of a Telstar LioQuest equipment at -50°C for 3 h. Afterwards they were lyophilised for 19 h at a temperature of -50°C under a vacuum of 0.2 mbar, so that to eliminate the water in the pores by sublimation. Before the MIP tests the samples were heated to 35°C for 2 h. The porosimeter used was a Micromeritics AutoPore

Series IV 9500, which applied a maximum injection pressure of 31900 psi, allowing the exploration of pore diameters between 0.007 and 500 µm. Prior to mercury injection the sample was outgassed by applying a vacuum of 50 µm-Hg. Afterwards the mercury injection pressure was increased from 0.36 to 31900 psi in 110 steps. To determine the extrusion branch of the curve, the pressure was released in 57 steps down to a pressure of 4.44 psi. A contact angle of mercury of 139° both on advancing and of receding on the clay surface was considered.

The mercury does not intrude the microporosity (pores of a size of less than 0.002 µm, according to the classification of Sing *et al*. 1985), but only the macroporosity and part of the mesopores. The percentage of pores not intruded by mercury includes not only those whose sizes are below 0.007 µm or above 500 µm, but also those whose entrance pore size is below that value or those isolated, even if the pores themselves are larger. The percentage of pores not intruded can be computed by comparing the actual void ratio of the samples (computed from their dry density and solid specific gravity measured by pycnometers) and the apparent void ratio calculated from mercury intrusion. Then, assuming that the percentage of pores not intruded in a clay corresponds entirely to the micropore size, the percentage of micropores can be estimated.

4.4 SMECTITE BASAL SPACING

X-ray profiles were registered in subsamples of the GBM and of the blocks to determine the smectite basal spacing. For that, the X-ray profiles of a sufficiently flat surface of small fragments of the subsamples were registered at room temperature without any previous treatment. An anticatode of Cu (CuK_α) radiation was used with a Philips model X'Pert-MPD diffractometer at 40 mA, 45 kV operating condition. X-ray diffraction (XRD) experimental profiles were obtained with a 0.1 mm entrance slit and a scanning rate of 0.02 °2θ/s. Data were collected from 0.2 to 30 °2θ. The position of the peaks was adjusted by using the quartz in the samples as an internal standard. A profile function was fitted to the observed intensities in order to obtain better peak parameters (peak position, net intensity and full width at half maximum (FWHM)) completely describing the measured scan. The pseudo-Voigt profile function, which is the weighted mean between a Lorentz and a Gaussian function, was used. This function was also used to deconvolute overlapped peaks.

4.5 THERMAL CONDUCTIVITY

The superficial thermal conductivity was measured with a Kemtherm QTM-D3 equipment of Kyoto Electronics that works according to the transient hot wire method (Kyoto Electronics 1987). In particular, the probe method, in which the wire is placed between the surface of the sample and an isolating material, was used.

The measurements were performed at room temperature, placing the probe on the surface of the sample, which must have a surface area of at least 10x4 cm and a depth of about 4 cm. The contact between the probe and the sample surface must be perfect, for which reason the sample surfaces were smoothed with a knife when necessary. Thermal conductivity was measured on blocks and on some GBM samples of the sampling section CMT3. In most of the GBM samples this was not possible due to their small size. The measurements were performed in the wrapped blocks, cutting the plastic film just enough to allow a good contact between the probe and the sample and protecting the whole set with plastic bags (Figure 10). When possible, the measurement was performed in two perpendicular positions in each block. Three measurements were performed in each position, and the value given is the average of these. The accuracy of the equipment is 3%.

Figure 10: Measurement of thermal conductivity on a bentonite block surface and on a GBM sample

4.6 HYDRAULIC CONDUCTIVITY

The hydraulic conductivity of GBM samples was measured according to a method developed at CIEMAT for expansive soils (CIEMAT procedure IMA/X8/BI-F14). The theoretical principle on which the method is based is that of the constant head permeameter. Basically, it consists in measuring against time the volume of water that passes through a specimen, confined in a rigid cell preventing it from deforming, to which a constant hydraulic gradient between the upper and lower parts is applied. The complete saturation of the sample and associated swelling guarantee perfect contact with the wall of the cell, preventing the flow of water between this and the sample.

The measuring system is made up of the following elements (Figure 11):

- Stainless steel cell with water inlet and outlet on bottom and top, respectively, in which the sample was confined. The internal dimensions of the sample were 19.63 cm^2 in surface area and a maximum length of 2.50 cm.
- An injection pressure system. An oil/water pump connected to the bottom of the sample was used for this purpose, with an intermediate deposit that separated the water in the pressure system from the Pearson water injected to the sample.
- A pressure system for the downstream pressure applied on top of the sample. A GDS pressure/volume controller was used for this purpose. The GDS controllers allow fixing of pressure with an accuracy of 1 kPa and measuring of water volume changes resolved to 1 mm^3. An intermediate deposit was also used to separate the water in the pressure system from the Pearson water injected to the sample. In a few cases an oil/water pump was used to apply the backpressure, with an automatic volume change apparatus, with an accuracy of 0.001 cm^3, used to measure the water outflow (Figure 12).
- Data acquisition system to record the water outflow.

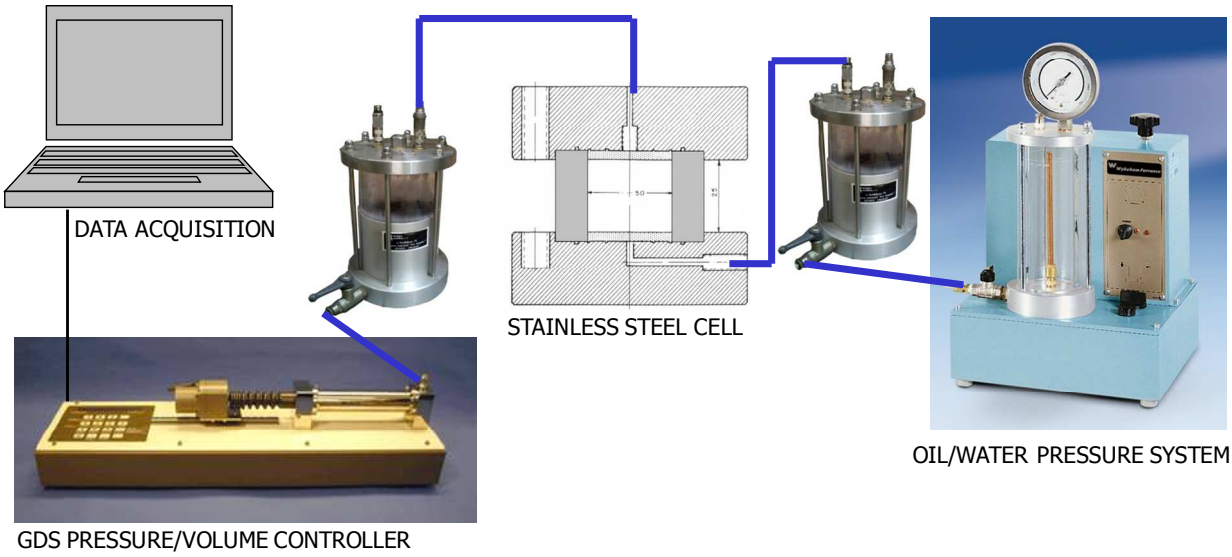

Figure 11: Schematic representation of the assembly for permeability measurement of expansive soils (with pressure volume controller to apply backpressure and measure outflow)

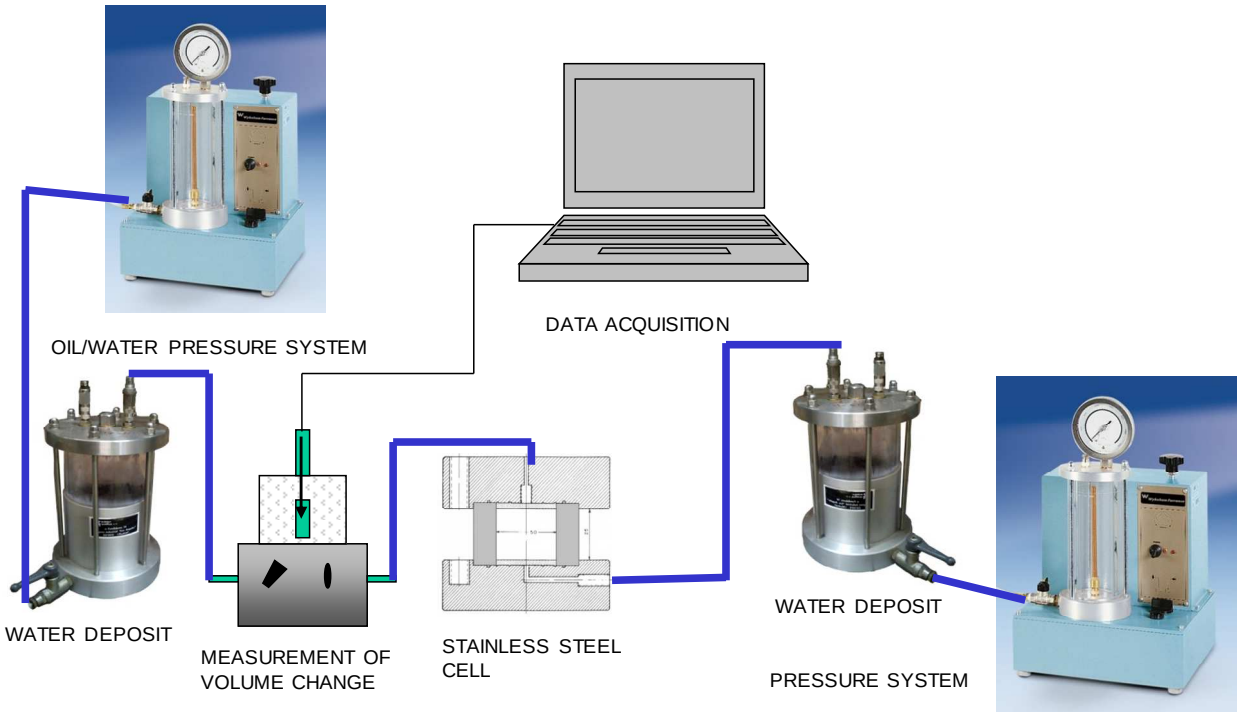

Figure 12: Schematic representation of the assembly for permeability measurement of expansive soils (with automatic volume change apparatus to measure outflow)

The specimens were obtained by trimming the samples of the GBM to the appropriate dimensions (cylinders of maximum height 2.5 cm and diameter 5.0 cm). This was done with knives and cutting rings, since the material was soft and easy to work with. Figure 13 shows the appearance of a sample during its preparation. Filter papers were placed in contact with the upper and lower parts of the sample, followed by porous stones.

Figure 13: Preparation of a sample for permeability determination

Once the covers of the cell were adjusted, the sample was saturated from both faces with Pearson water injected at a pressure of 600 kPa. In this way the sample was hydrated to complete saturation over the necessary time period, which was between 8 and 24 days. This was checked by measuring the water intake.

Once the sample saturated, a hydraulic head was applied by modifying either the injection or the backpressure. The hydraulic head is the difference between the upstream and downstream pressures ($\Delta P = P_i - P_b$) and gives place to a supposedly linear hydraulic gradient, which is the ratio existing between the hydraulic head and the length of the specimen. The range of pressures used was between 400 and 12000 kPa, which produced hydraulic gradients between 500 and 3500. The water volume passing through the sample was measured online. The tests run over a time period sufficient to determine that the volume of water passing through the specimen was linear and stable with time for a given hydraulic gradient.

Once constant flow was achieved, the volume of water passing through the sample (ΔV, cm^3) was determined over a given time period (Δt, s). Hydraulic conductivity k_w (cm/s) was calculated by applying Darcy's law for flow in porous media:

$$k_w = \frac{\Delta V \times l}{A \times \Delta t \times \Delta P} \qquad [7]$$

where ΔP is the hydraulic head in cm of water, A is the surface area of the cell (19.63 cm^2) and l the length of the specimen (in cm).

The tests were performed at room temperature. At the end of the test, the sample was weighed, measured and oven-dried at 110°C to check the actual water content and dry density.

Additionally, three tests were performed in high-pressure oedometer equipments (Figure 14). The samples were obtained by trimming as explained above to fit the oedometer rings, which had an inner diameter of 5.0 cm, the length of the resulting specimens being about 2 cm. The specimens thus obtained were confined between porous stainless steel sinters. The oedometer assemblage was placed in the oedometric frame and a small vertical load was applied to the sample to assure a good contact with the load cell installed in the loading frame, and further deformation of the sample was hindered by means of setscrews. The sample was hydrated at constant volume through the top and bottom surfaces with Pearson water injected initially at a pressure of 0.01 MPa and then at 0.6 MPa. At the same time, the load cell measured the swelling pressure exerted by the clay (see next section). The small vertical deformation of the

specimen, due mainly to the load cell and frame deformability, was measured by LVDTs. The water intake during saturation was measured by a volume change apparatus. Two intermediate deposits were used on top and bottom to separate the Pearson water in contact with the sample from the deionised water used in the pressure systems. The values of load, strain and water exchange were automatically recorded.

Once the sample was completely saturated (which was assumed by the stabilisation of swelling pressure development), hydraulic conductivity was determined in the same equipment and on the same samples, which were kept at constant volume. In order to perform this determination, the water pressure at the bottom of the samples was increased to 1000 or 1200 kPa, while a backpressure of 600 kPa was applied on top, or the backpressure on top was reduced to 300 or 400 kPa while the injection pressure was kept in 600 kPa. This resulted in hydraulic gradients between 1000 and 1900. The water outflow was measured by a volume change apparatus and the hydraulic conductivity (k_w) was calculated applying Darcy's law (Equation 7).

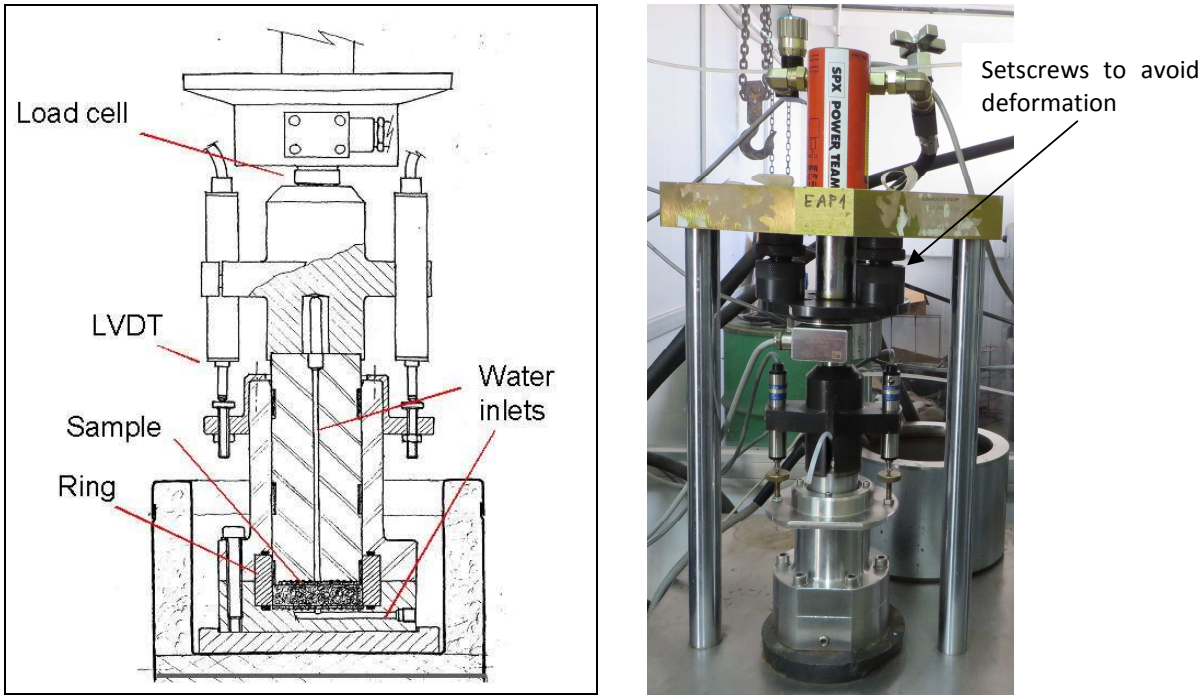

Figure 14: Schematic layout and appearance of the high-pressure oedometric cell

4.7 SWELLING PRESSURE AND SWELLING CAPACITY

On a small number of samples two kinds of tests were performed to determine the swelling capacity of the GBM, namely, swelling pressure tests and swelling deformation test (swelling under load). Four swelling deformation tests and a swelling pressure test were performed in standard oedometers at laboratory temperature. Three other swelling pressure tests were performed in the high-pressure oedometers described above (Figure 14), prior to the determination of hydraulic conductivity. For both kinds of tests the specimens were prepared by trimming the GBM samples with a knife and a cutting ring to fit the oedometer rings. The oedometer ring prevented the sample, which was confined between two porous stones or stainless steel sinters at its upper and lower surfaces, from deforming laterally. In the tests performed in standard oedometers the initial height of the specimens was 1.2 cm and their section was 11.4 cm^2, whereas in those tests performed in the high-pressure oedometers the initial height of the specimens was 2.0 cm and their section was 19.6 cm^2.

In the swelling deformation tests, a vertical pressure of 0.02, 0.4 or 0.5 MPa was applied to the samples once in the oedometer. Immediately afterwards, the samples were flooded with deionised water at atmospheric pressure from the bottom porous plate. The swelling strain experienced by the specimens upon saturation was recorded as a function of time until stabilisation. The final result is the percentage of strain of a sample of given initial dry density and water content on saturating under a fixed load. On completion of the test, the water content of the specimen was determined.

The swelling pressure test makes it possible to determine the equilibrium swelling pressure exercised by a sample on complete saturation at constant volume. For the swelling pressure test performed in a standard oedometer, once the sample was placed in the oedometer cell, the lower porous stone was covered with deionised water, such that the sample began to saturate from the bottom upwards, allowing the air in the pores to escape through the upper part. The sample volume was kept constant during saturation by applying the necessary loads by means of a system of levers. The swelling pressure exercised by the sample was determined from the load that had to be applied in order for the volume of the sample to be kept constant during saturation. Swelling pressure tests are usually considered to be completed when, under a constant vertical load, no strain is observed for at least 24 h.

Three other swelling pressure tests were performed in the high-pressure oedometer described in section 4.6. The specimens used in this case were larger, and they were saturated simultaneously through top and bottom with Pearson water instead of deionised water. Since an injection pressure of up to 0.6 MPa was applied to saturate the samples, this had to be taken off from the equilibrium pressure value recorded by the load cell. Final water content and dry density were checked upon dismantling.

5 Results

5.1 DRY DENSITY AND WATER CONTENT

The samples for the water content and density determinations were taken following approximately sampling radii in the sampling sections. They were prepared by trimming regular specimens with volumes of between 6 and 13 cm^3. A detailed report of these measurements was given in Villar (2013), and the values obtained for each sample are given in Appendix 1.

The water contents determined in the laboratory ranged between 33 and 43% and the dry densities between 1.42 and 1.24 g/cm^3, with a clear trend for the water content to increase and the dry density to decrease towards the bottom part of the barrier (Figure 15). The deviations with respect to the average values were higher towards the bottom of the GBM because the increase in water content towards the bottom was sharper in the lower part of the GBM. There were differences among sections in the GBM, and the average water content of the GBM increased towards the bottom part of the gallery (from section CMT1 to CMT3). The comparison between the values obtained on site and in the laboratory showed a very good agreement.

The blocks had water contents similar to those of the adjacent GBM, between those of the bottom and the upper part of the GBM, and their density had decreased from an initial value of 1.7 g/cm^3 to values close to 1.4 g/cm^3, similar to the average dry density of the GBM. The average values were similar for all the sampling sections.

The degrees of saturation of the barrier were homogeneous, ranging between 95 and 101%. It is considered that the average pore water density in the barrier was close to 1.0 g/cm^3 due to the low dry density of the bentonite.

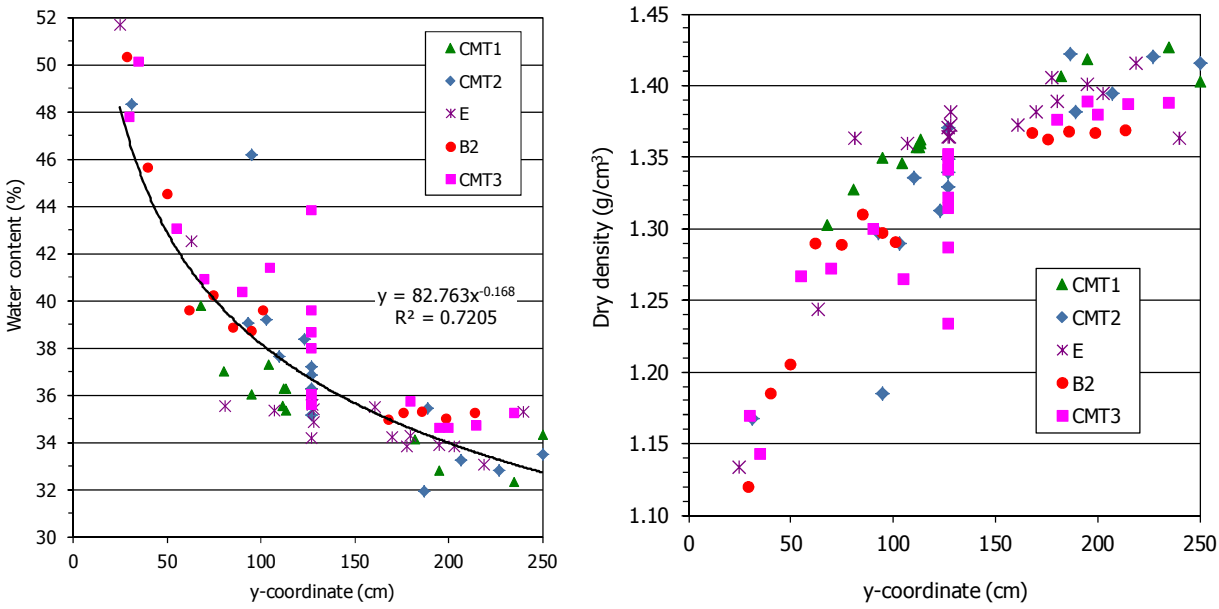

Figure 15: Water content and dry density measured in the GBM of different sections as a function of the distance to the bottom part of the gallery (Villar 2013)

5.2 SUCTION MEASUREMENT

The suction of the samples was computed with Equation 5 from the relative humidity and temperature measured in the laboratory in samples of the blocks and the GBM (values for each sample given in Appendix 1). The values obtained with the psychrometers, which ranged between 2.1 and 4.7 MPa, are plotted in Figure 16 as a function of the water content of the bentonite for the different kinds of samples. Despite the large dispersion, the suction is seen to decrease with water content, and no difference could be found between the GBM and the blocks. The relationship between suction and dry density was inverse, but no clear relation with the degree of saturation could be verified (Villar 2013).

Figure 17 shows the suction values measured in the EB samples as a function of their water content and the empirical fittings obtained with Equation 4 for three different dry densities: the average of all the samples in which suction was measured (1.34 g/cm^3), the highest (1.43 g/cm^3) and the lowest density (1.12 g/cm^3). It is clear that the suctions measured in the samples retrieved are higher than the values expected for FEBEX samples of the same dry density and water content. The reason could be that the samples from the EB were saturated with saline water and would consequently have a high osmotic suction, whereas the samples with which the empirical correlation was obtained had been saturated with deionised water.

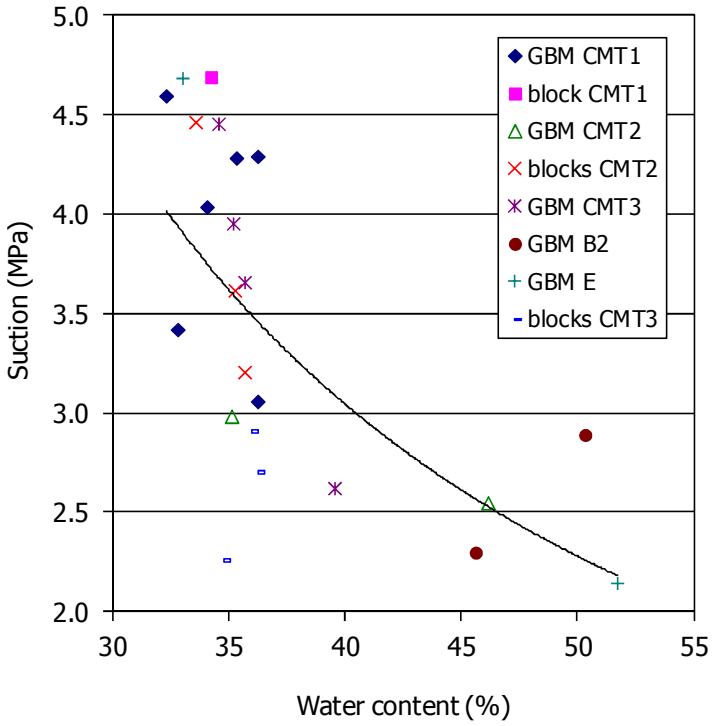

Figure 16: Suction computed from the psychrometer measurements in samples from different sampling sections as a function of the water content of the samples (Villar 2013)

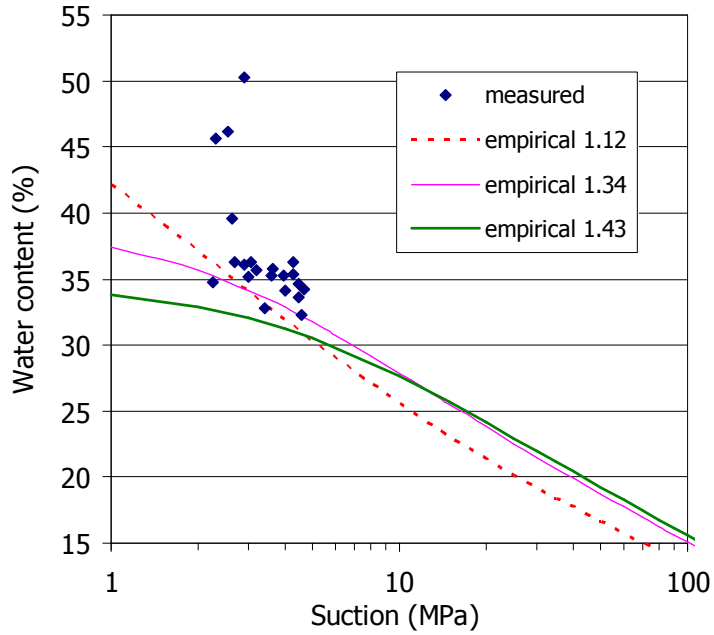

Figure 17: Suction values measured with psychrometers in the samples retrieved and empirical fittings for FEBEX bentonite at different dry densities (indicated in g/cm^3) obtained with Equation 4

5.3 PORE SIZE DISTRIBUTION

The pore size distribution of lyophylised fragments of the EB samples was determined by mercury intrusion porosimetry (MIP) and the results obtained for each sample are presented in Appendix 2. Assuming that the percentage of pores not intruded in a clay corresponds entirely

to the <7 nm size, an estimation of the percentage of micropores was computed and the percentage of each pore size recalculated. The percent of the porosity intruded by the mercury was fairly low (between 50 and 60%), this meaning that there was an important volume of pores with a size of less than 7 nm or not interconnected, that have been considered micropores. Figure 18 shows the pore size distribution in terms of incremental pore volume for the GBM samples of four sections. The pore size distribution determined by MIP showed that during operation the GBM developed a macropore family with diameters between 3 and 35 µm that did not exist in the original material. However, most of the porosity of the samples analysed, around 50%, belonged to the microporosity size (less than 7 nm, Figure 19), except for those samples of dry density below 1.3 g/cm^3. In these low dry density samples the macropore familiy was the predominant one and the macropore size was inversely related to the dry density of the bentonite (Figure 20).

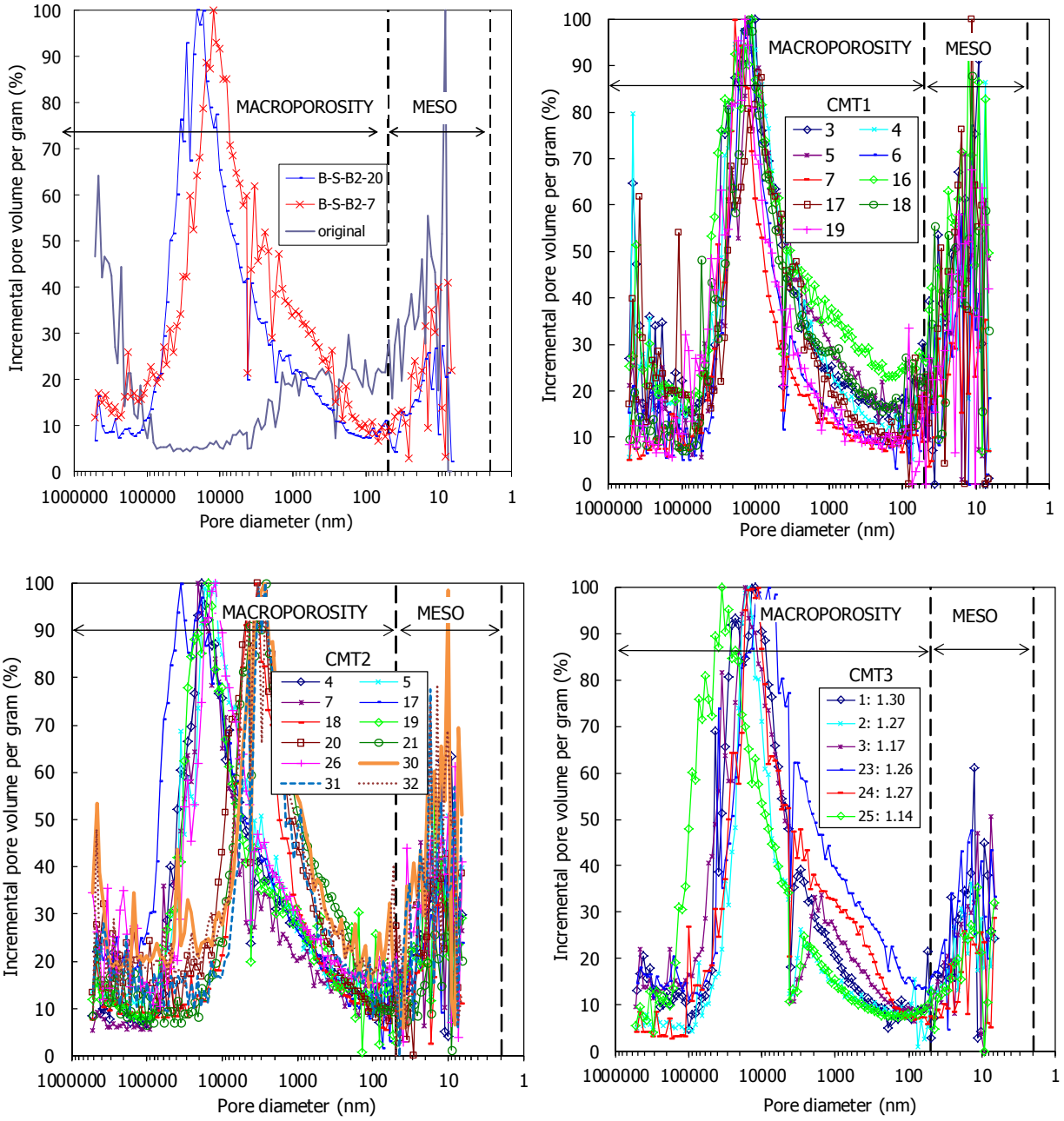

Figure 18: Incremental pore volume for GBM samples (samples B-S) of four sampling sections. In the first Figure the curve for the original material is shown and in the last Figure the dry density of the samples is indicated in g/cm^3

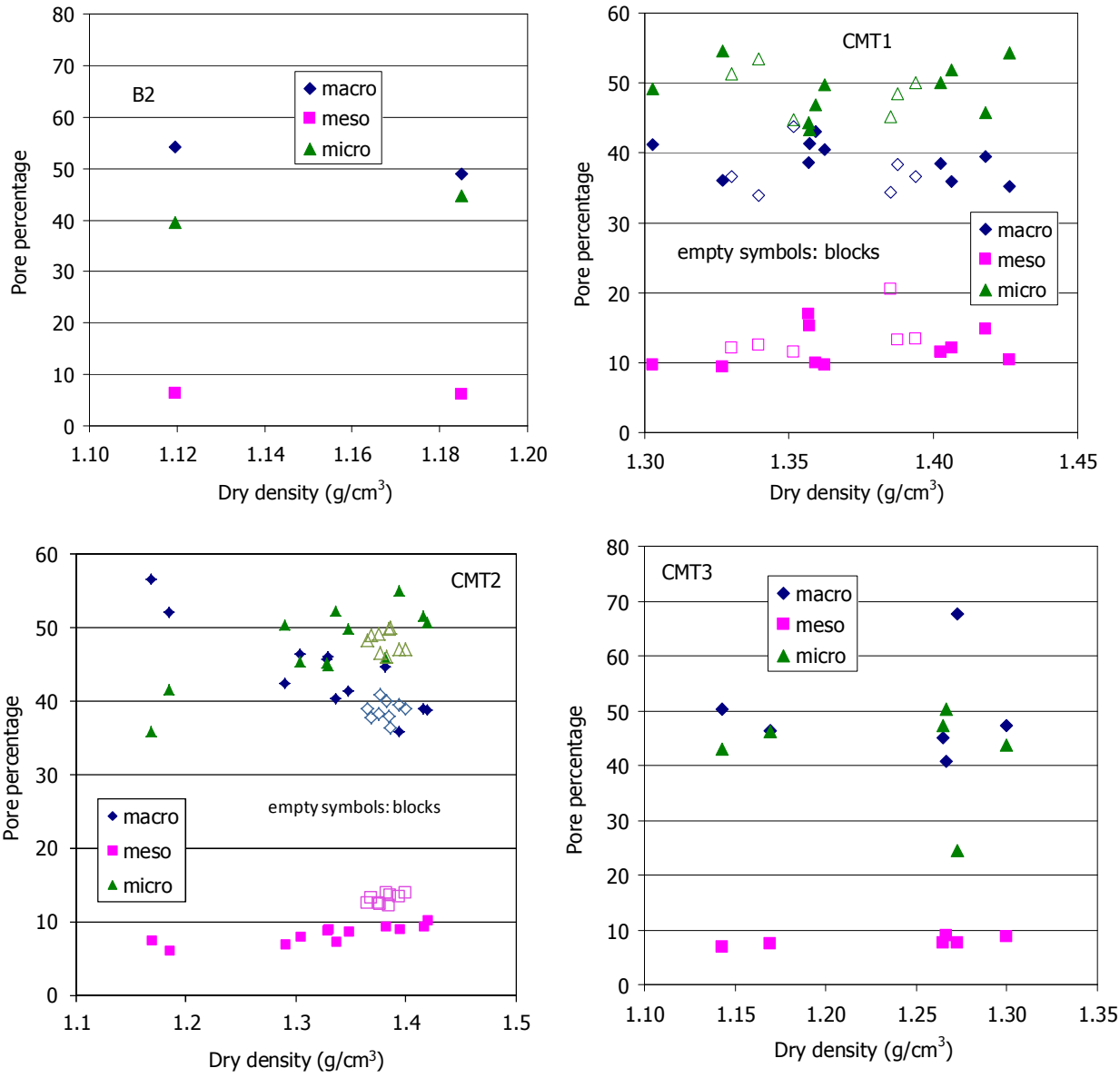

Figure 19: Pore size distribution of samples from the different sampling sections

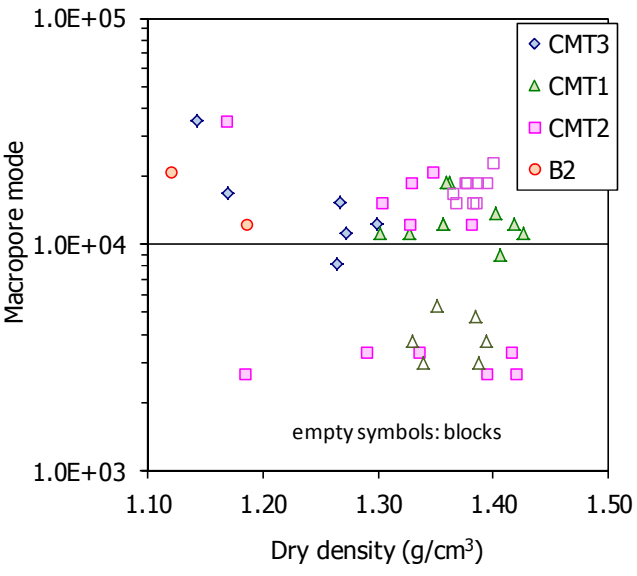

Figure 20: Mode of macropores as a function of dry density for samples of different sections

The comparison between samples of the GBM and of the blocks does not allow drawing clear conclusions. Thus, in section CMT1 the block samples had systematically a mode of macropores lower than the GBM, whereas in section CMT2 the contrary happened (Figure 21).

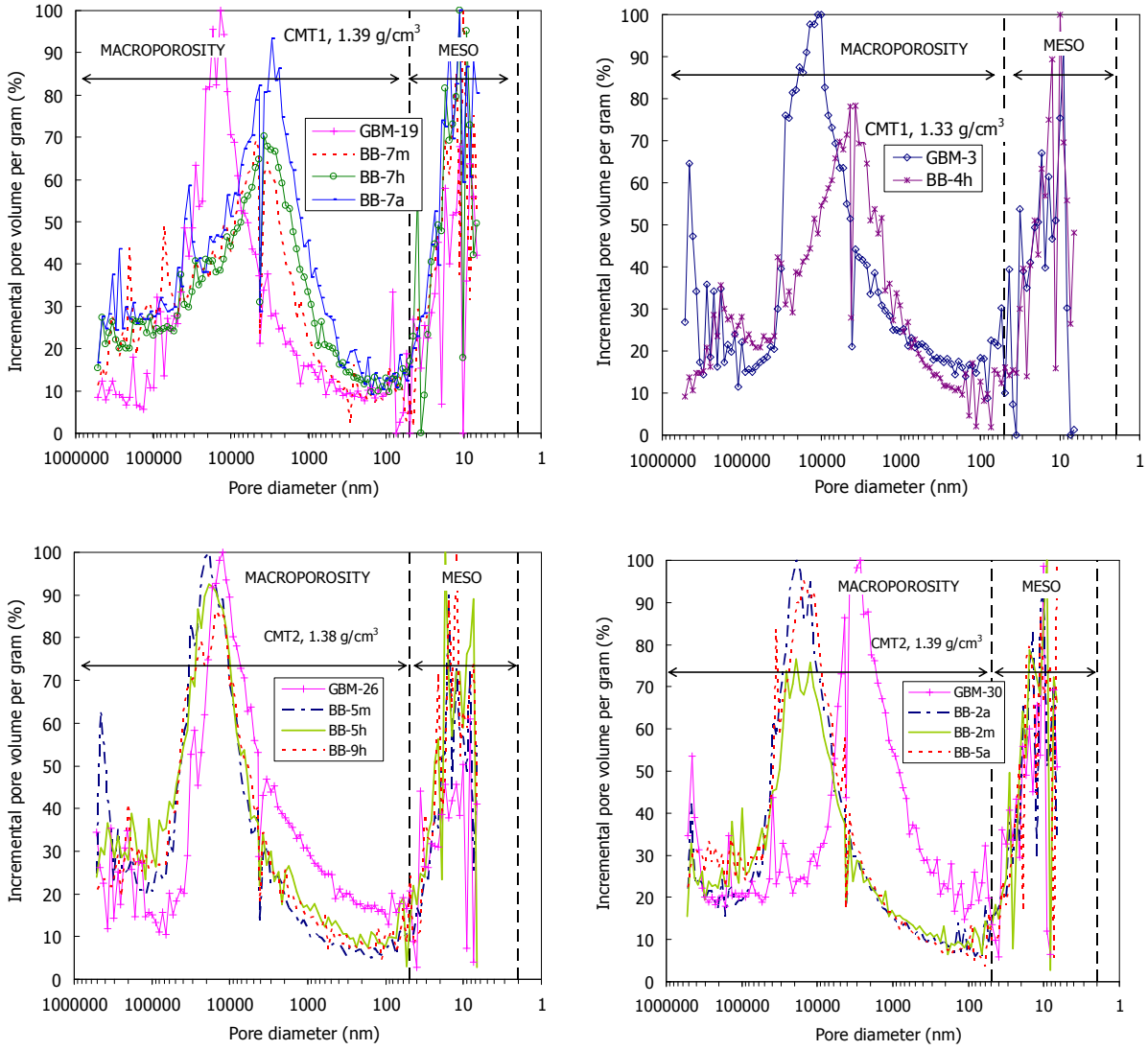

Figure 21: Comparison of the pore size distribution of samples of blocks (BB) and GBM (samples B-S) of the same dry density in sections CMT1 (up) and CMT2 (bottom)

5.4 SMECTITE BASAL SPACING

X-ray profiles were registered in some EB samples to determine the smectite basal spacing. For that, the X-ray profiles of a sufficiently flat surface of the samples were registered at room temperature without any previous treatment. The values obtained, both for GBM and block samples, are given in the Tables of Appendix 1 and plotted in Figure 22. Block samples were analysed only in sections CMT1 and CMT2, but there is not a clear distinction between the results obtained for the two kinds of samples (Figure 23). For water contents approximately below 38%, the basal spacing increased with the water content, but for higher values the basal spacing did not seem to depend on the water content. Also, samples from section CMT3 tended to present higher basal spacings than samples of the same water content taken in other sections. For most of the samples the basal spacings of the smectite indicate that 3 water layers were completely developed in the interlayer (values around 1.85 nm). In fact, for many samples the *d*(001) peak was a double one that could be deconvoluted in two peaks, the one shown in

the Figures and another one towards lower angles, i.e. higher spacings. The two peaks could be told apart by profile fitting of the XRD pattern. An example of this is shown in Figure 24.

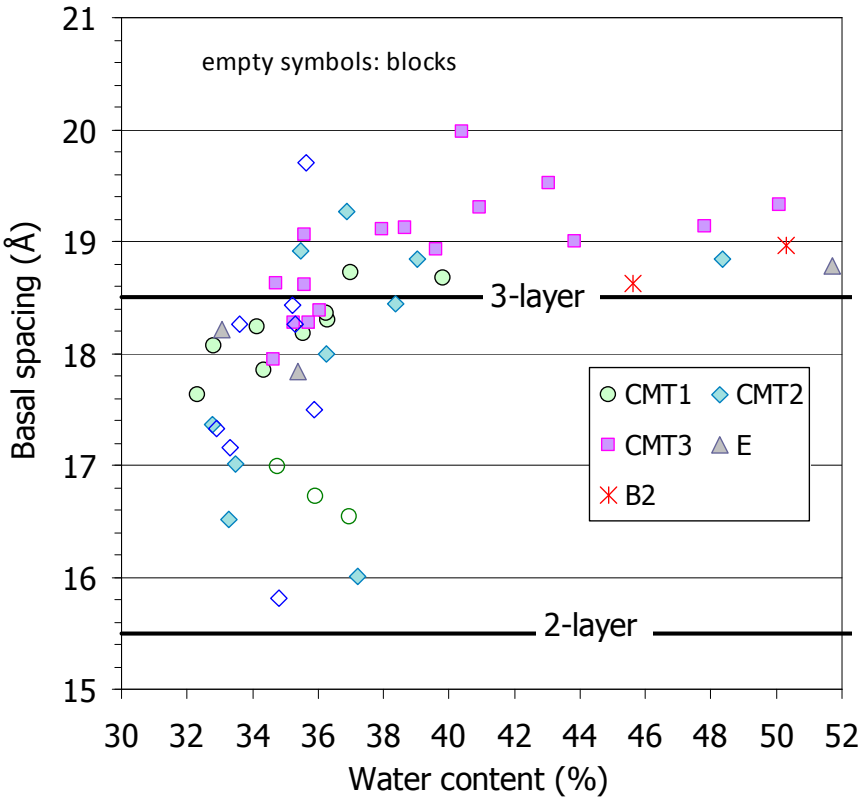

Figure 22: Basal spacing of the smectite in EB samples of different sections

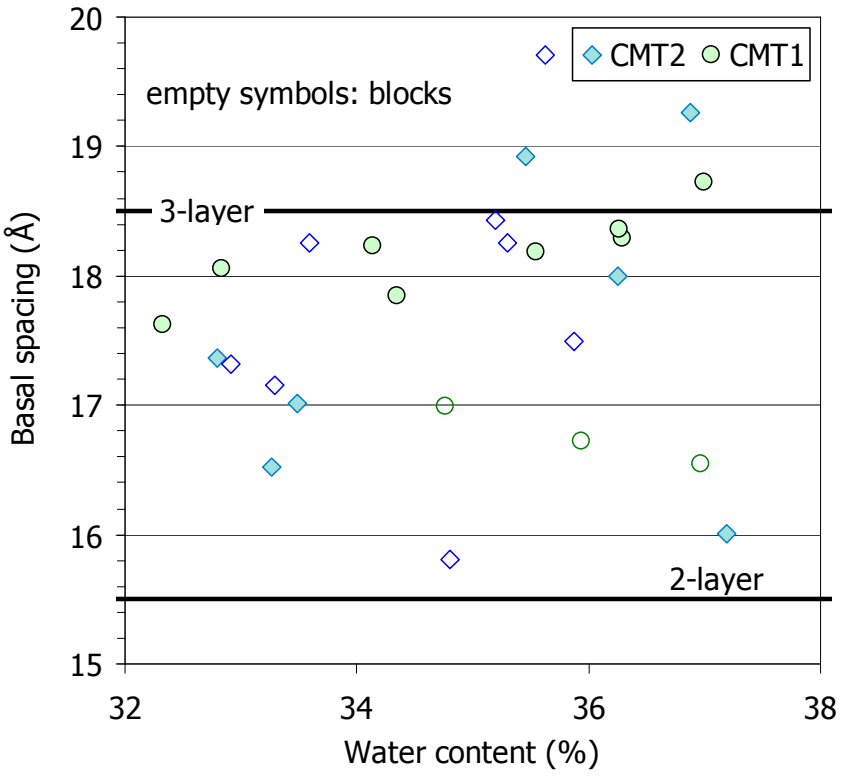

Figure 23: Basal spacing of smectite in samples from sections CMT1 and CMT2 (blocks and GBM)

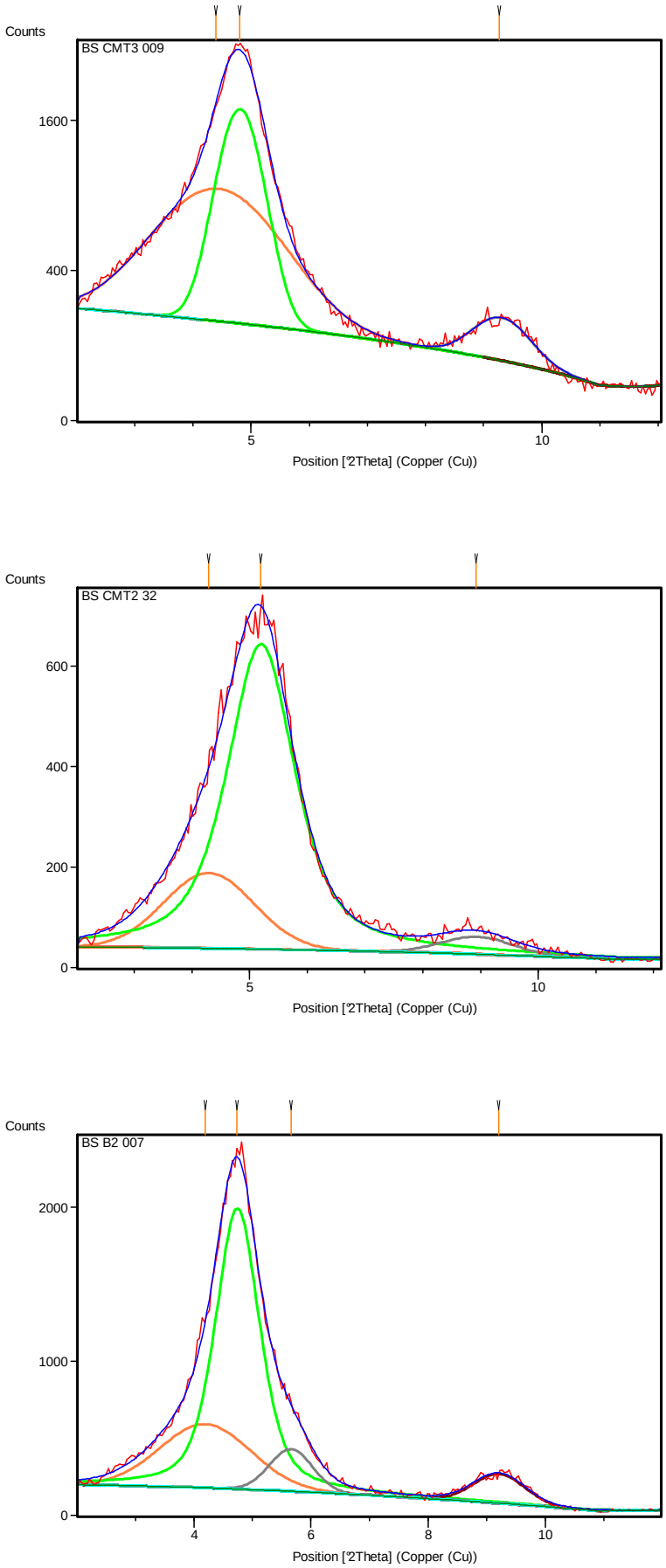

Figure 24: Profile fitting of the XRD pattern of samples B-S-CMT3-009 (up, peaks at 20.08 and 18.38 Å), B-S-CMT2-32 (middle, peaks at 20.59 and 17.01 Å) and B-S-B2-007 (down, peaks at 21.06 and 18.62 Å) (Gutiérrez-Nebot 2013)

The average values of the two deconvoluted peaks have been plotted along with values obtained for the FEBEX bentonite saturated in different ways with deionised water (Villar et al. 2012a) and are shown in Figure 25. Some of the samples saturated in laboratory tests with deionised water were pellets mixtures similar to the GBM material used in the EB test (Villar 2012), but most of them were samples obtained from compaction of the granular material to a wide range of dry densities (from 1.1 to 1.75 g/cm^3). The values obtained for the EB samples for water contents higher than 38% are similar to what was observed for FEBEX bentonite samples of the same water content saturated with deionised water, or even higher. However, for water contents below this value, the basal spacings measured in the EB samples are lower than those measured in samples prepared in the laboratory. The dispersion of values for a given water content for the EB samples is very large though, and strong conclusions cannot be drawn. It is acknowledged that the time from sampling to XRD analysis was longer for the EB samples than for the samples prepared in the laboratory, which is why some drying could have taken place in the EB samples before the measurement, which could have implied a decrease in basal spacing that has not been assessed.

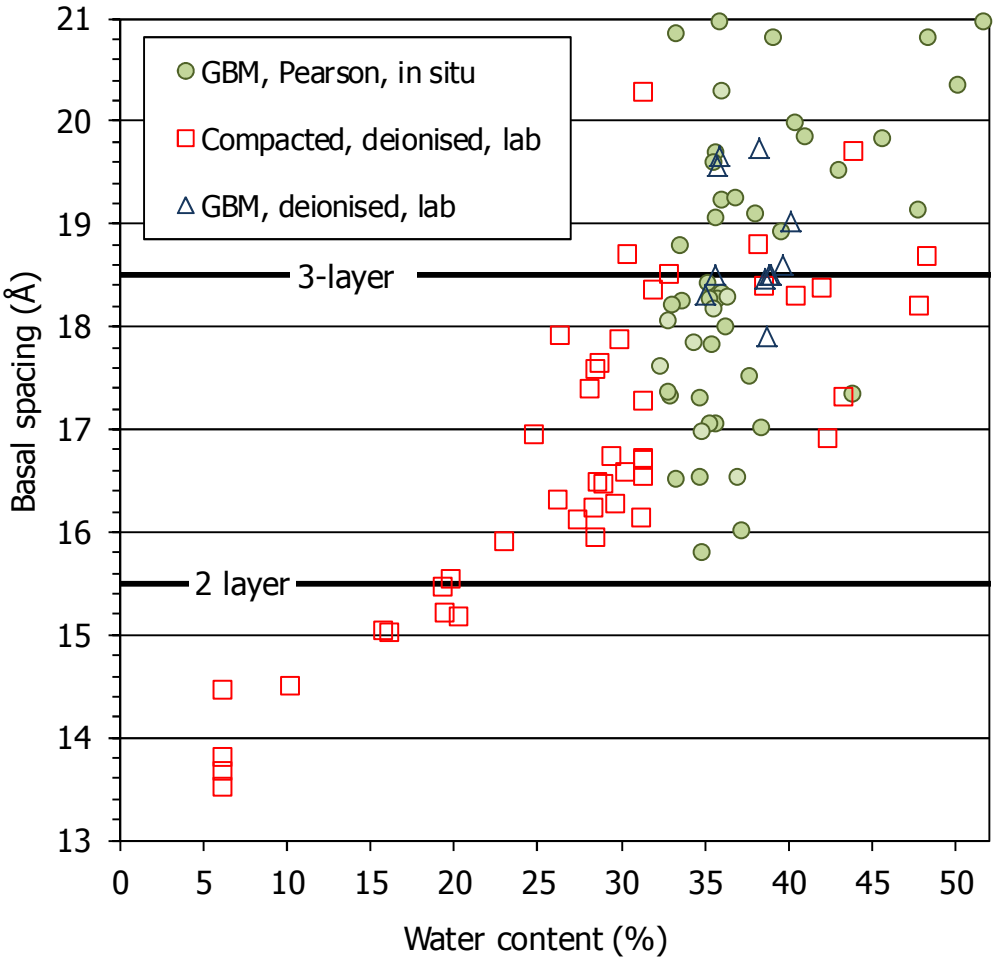

Figure 25: Basal spacings of FEBEX samples saturated in different ways with deionised water (Villar et al. 2012a) and of samples from the EB test

5.5 THERMAL CONDUCTIVITY

The superficial thermal conductivity was measured at room temperature using the transient hot wire method on blocks of several sections and on GBM samples of the sampling section CMT3, as detailed in Appendix 1. The values obtained were between 0.9 and 1.35 W/m·K, and

when plotted as a function of the y-coordinate, they tended to increase towards the bottom of the gallery (0 y-coordinate), with lower thermal conductivities for the GBM than for blocks located at the same position (Figure 26). The relation of the thermal conductivity values with dry density and water content is not straightforward, and for a given water content, a range of thermal conductivities was measured (Figure 27). This is probably due to the fact that all the samples had a high degree of saturation, and it was checked during FEBEX that for degrees of saturation close to 100%, dry density did not affect noticeably thermal conductivity (Villar 2002, ENRESA 2006). Only the samples with dry densities well below the average (and water contents above), had clearly a lower thermal conductivity, which could indicate that the contribution of water content to the increase in thermal conductivity was lower than the reduction of thermal conductivity associated with the decrease in dry density. Nevertheless, the thermal conductivity measured on the samples from the EB was lower than that measured on samples of untreated FEBEX bentonite compacted to degrees of saturation close to 100% (Figure 28).

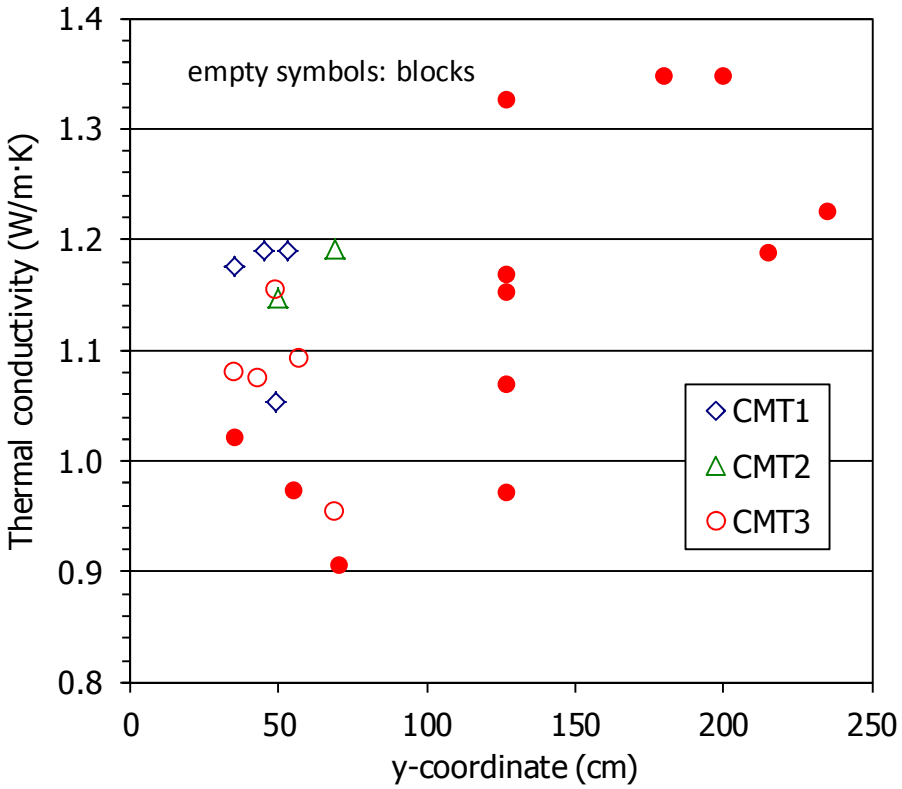

Figure 26: Thermal conductivity measured on blocks and GBM samples (y-coordinate is the distance to the bottom of the gallery)

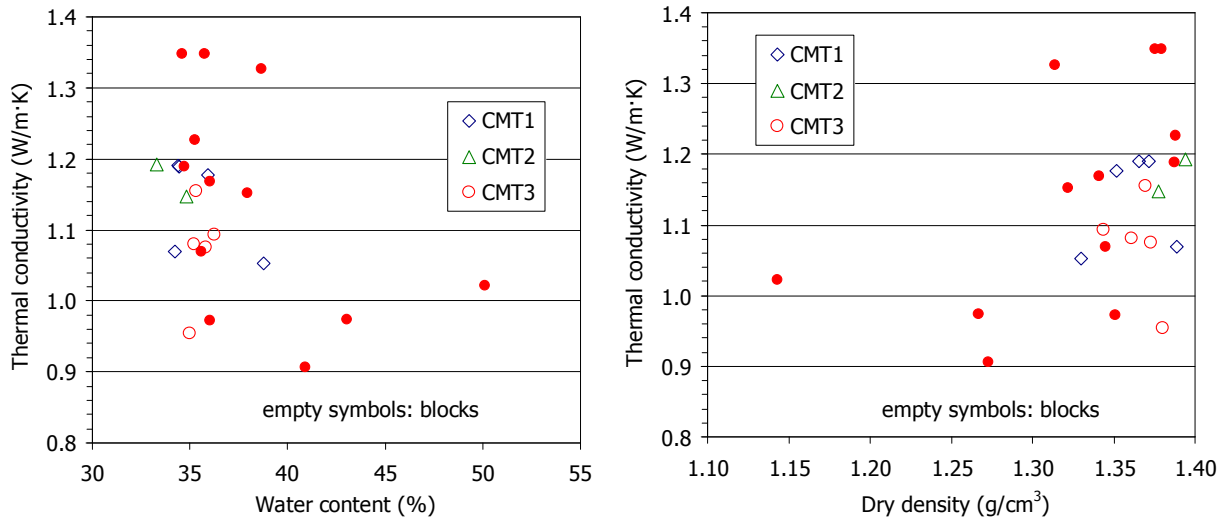

Figure 27: Thermal conductivity of blocks and GBM as a function of their water content and dry density

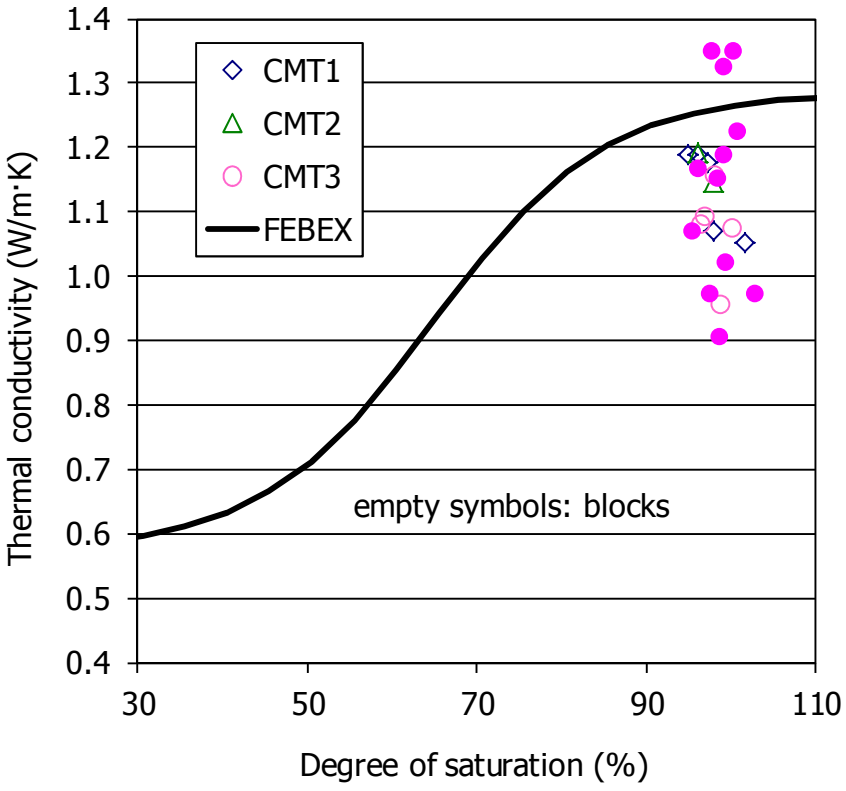

Figure 28: Comparison of thermal conductivity measured in EB samples and empirical correlation for untreated FEBEX blocks (Eq. 5)

5.6 HYDRAULIC CONDUCTIVITY

The hydraulic conductivity was measured in cylindrical samples of the GBM trimmed to fit the permeability cells. The samples were initially saturated through both sample surfaces with Pearson water injected at 600 kPa. The water intake during the saturation process, which took between 8 and 24 days, was of between 2 and 5 cm^3. It must be pointed out that, although the samples had a very high initial degree of saturation, they took water because, once in the cell,

their density decreased with respect to the original value, due to the filling of some irregularities that could have been created during trimming.

After saturation a hydraulic gradient of between 500 and 3500 was applied and kept until the outflow rate was constant. Afterwards, the hydraulic gradient was changed and kept until constant outflow rate. The whole measuring process took between 8 and 46 days. As an example, the outflow curves for some samples and hydraulic gradients are shown in Figure 30. These flows were used to compute permeability using Equation 7. The values obtained for all the samples have been plotted in Figure 31 as a function of the hydraulic gradient applied. Lower hydraulic gradients gave place in some cases to slightly lower permeabilities.

Figure 29 shows the appearance of GBM samples at the end of the permeability tests, they looked homogenous, sometimes with black spots and occasionally with small cavities that the swelling of the bentonite did not seem enough to fill. The degrees of saturation checked upon dismantling of the cells were slightly above 100%. A summary of the characteristics of all the tests, including the average permeability value obtained for the measurements performed under two different hydraulic gradients is given in Table III.

These average hydraulic conductivity values have been plotted in Figure 32 as a function of the final dry density inside the cell. The theoretical curve for FEBEX granular bentonite permeated with deionised water (Equation 1) and its range of variation are also shown in the Figure. The hydraulic conductivities measured in the GBM samples retrieved were in the range from $8 \cdot 10^{-12}$ to $2 \cdot 10^{-13}$ m/s. These values were determined using Pearson water as fluid. When comparing these values to those expected for untreated FEBEX bentonite of the same dry density permeated with deionised water, it was found that the values for the GBM were slightly above (a 12%) the theoretical ones, but almost for all the cases inside the expected range of variation of this property for FEBEX bentonite. This increase can be attributed to the different salinity of the water used with the retrieved samples, since a higher salinity would increase permeability (Castellanos et al. 2008). Consequently, it is considered that the permeability of the GBM did not change during operation.

Figure 29: Appearance of B-S samples after the permeability tests

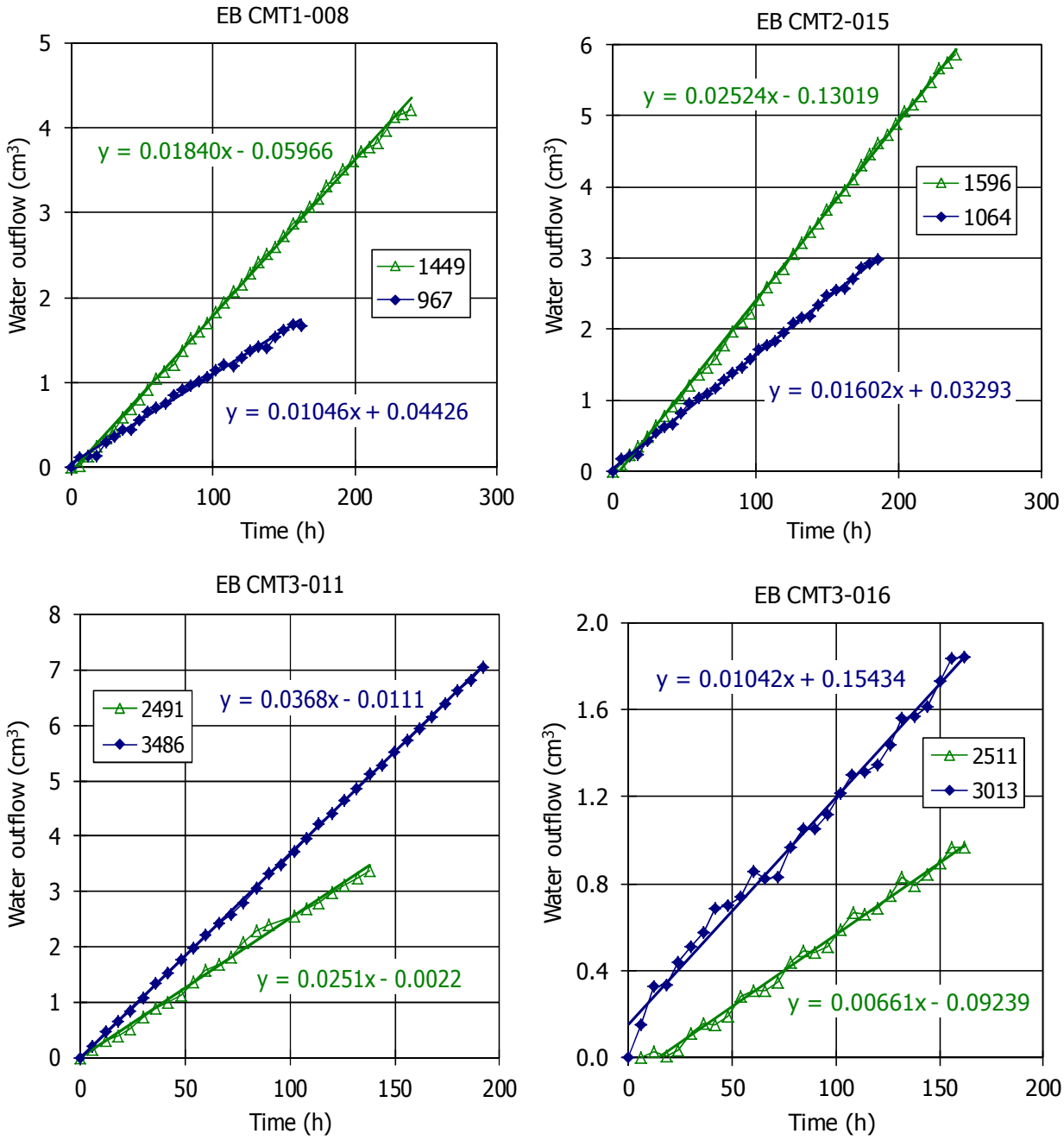

Figure 30: Water outflow during some of the permeability tests with GBM samples (samples B-S). The hydraulic gradients applied are indicated in the legends

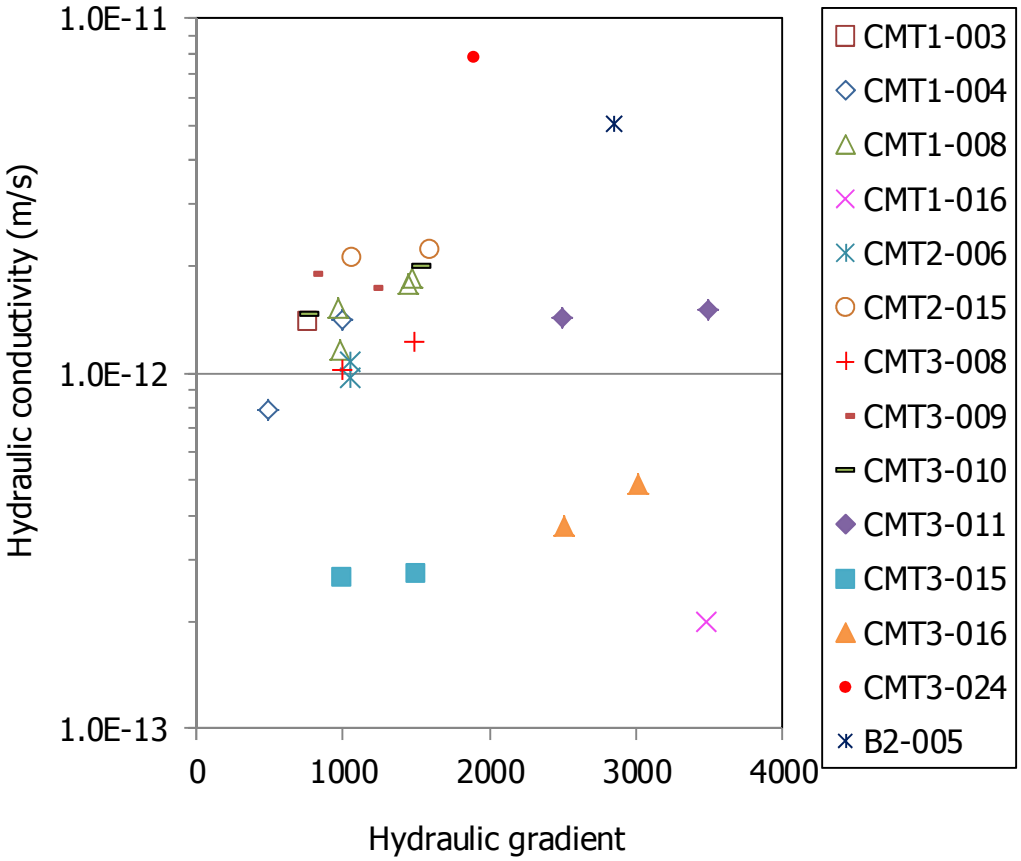

Figure 31: Hydraulic conductivity of B-S samples as a function of the hydraulic gradient applied

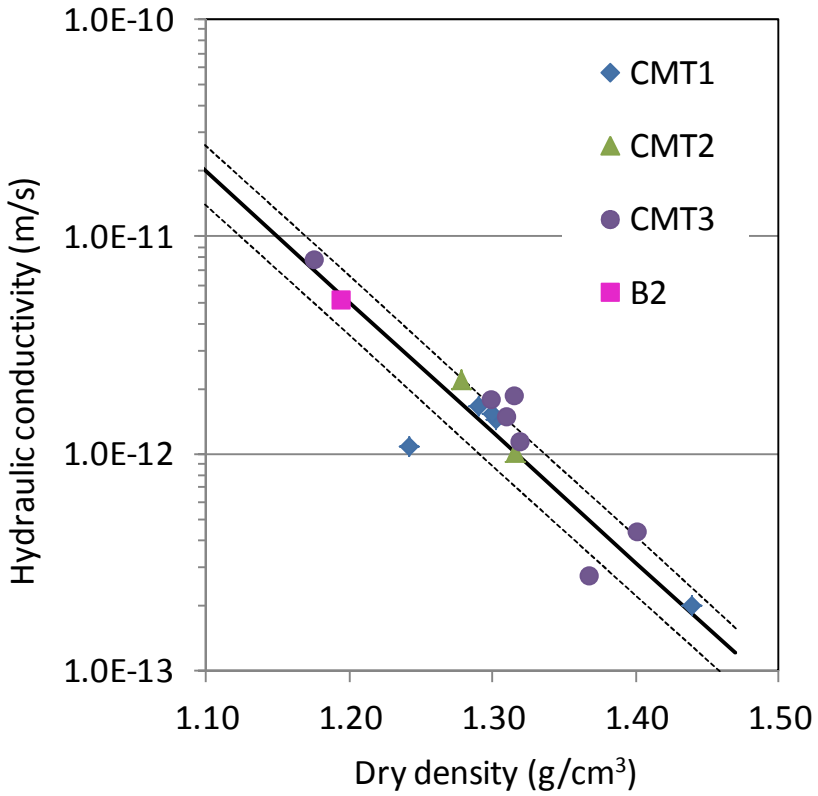

Figure 32: Hydraulic conductivity determined with Pearson water in samples retrieved upon dismantling of the EB test (B-S samples) and empirical correlation for untreated FEBEX bentonite (Eq. 1)

Table III: Summary of the hydraulic conductivity tests performed in B-S samples

Reference	Initial ρ_d (g/cm^3)	Initial w (%)	Initial S_r (%)	Final ρ_d (g/cm^3)	Final w (%)	Final S_r (%)	k_w [b] (m/s)	T (°C)
CMT1-003	35.6	1.35	96	39.3	1.30	99	$1.4 \cdot 10^{-12}$	22.6
CMT1-004	40.1	1.29	99	43.9	1.24	101	$1.1 \cdot 10^{-12}$	22.0
CMT1-008[a]	35.4	1.35	96	40.4	1.30	101	$1.5 \cdot 10^{-12}$	25.0
CMT1-008	40.4	1.28	99	41.1	1.29	102	$1.7 \cdot 10^{-12}$	24.1
CMT1-016	31.7	1.45	99	34.3	1.44	106	$2.0 \cdot 10^{-13}$	21.1
CMT2-006	36.3	1.35	98	39.3	1.32	101	$1.0 \cdot 10^{-12}$	24.8
CMT2-015	39.1	1.30	98	41.5	1.28	101	$2.2 \cdot 10^{-12}$	24.1
CMT3-008	36.6	1.35	98	38.6	1.32	100	$1.1 \cdot 10^{-12}$	24.1
CMT3-009	36.5	1.34	97	40.0	1.32	103	$1.8 \cdot 10^{-12}$	24.1
CMT3-010	38.0	1.31	97	40.7	1.30	102	$1.7 \cdot 10^{-12}$	23.0
CMT3-011	37.1	1.35	99	39.4	1.31	100	$1.5 \cdot 10^{-12}$	21.7
CMT3-015	34.7	1.40	100	36.8	1.37	102	$2.7 \cdot 10^{-13}$	23.8
CMT3-016	32.3	1.42	97	34.8	1.40	102	$4.3 \cdot 10^{-13}$	22.4
CMT3-024[a]	40.9	1.18	85	48.8	1.18	102	$7.7 \cdot 10^{-12}$	22.3
B2-005[a]	40.9	1.27	98	51.7	1.19	111	$5.0 \cdot 10^{-12}$	23.0

[a] determined in the high-pressure oedometer; [b] average of two measurements

5.7 SWELLING PRESSURE AND SWELLING CAPACITY

Four swelling under load tests were performed in GBM samples of section CMT3, and the characteristics of them are summarised in Table IV. As expected, the initial degrees of saturation of all the samples were very high, but all the samples took water during the tests and reached final degrees of saturation of 100%. The samples saturated under vertical loads close to 0.5 MPa experienced some decrease in dry density during the tests, but the sample tested under a very low vertical load (B-S-CMT3-019) swelled considerably, their dry density and water content changing substantially. The swelling process took long in all cases, particularly in the last one mentioned (Figure 33), which can be explained by the chemical changes that probably occurred during saturation in the oedometer, since the Pearson water initially in the pores of the specimens reacted with the deionised water used to saturated the samples, causing possibly changes in the DDL and the cation exchange complex.

The final deformation values obtained have been compared in Figure 33 (right) with the values obtained with the empirical Equation 3 for samples of untreated FEBEX of the same initial dry density and water content saturated under the same vertical loads with deionised water. In the three samples saturated under higher vertical loads, the swelling of the EB samples is lower than expected, whereas the sample saturated under a very low vertical load swelled more than predicted by the Equation. Perhaps the shorter tests did not run for long enough to allow for a chemical equilibrium, and the values measured corresponded to deformations obtained for slightly saline water, which could be why they were lower.

Table IV: Summary of the swelling under load tests performed in B-S samples with deionised water

Reference	Vertical pressure (MPa)	Initial ρ_d (g/cm^3)	Initial *w* (%)	Initial S_r (%)	Final ε (%)	Duration (days)	Final *w* (%)	Final ρ_d (g/cm^3)	Final S_r (%)
CMT3-008	0.55	1.35	36.4	98	-1.9	23	40.3	1.33	105
CMT3-009	0.43	1.34	35.4	94	-1.6	11	39.1	1.32	100
CMT3-015	0.43	1.39	33.8	96	-3.5	30	39.3	1.34	105
CMT3-019	0.02	1.32	37.2	96	-22.5	77	57.2	1.08	103

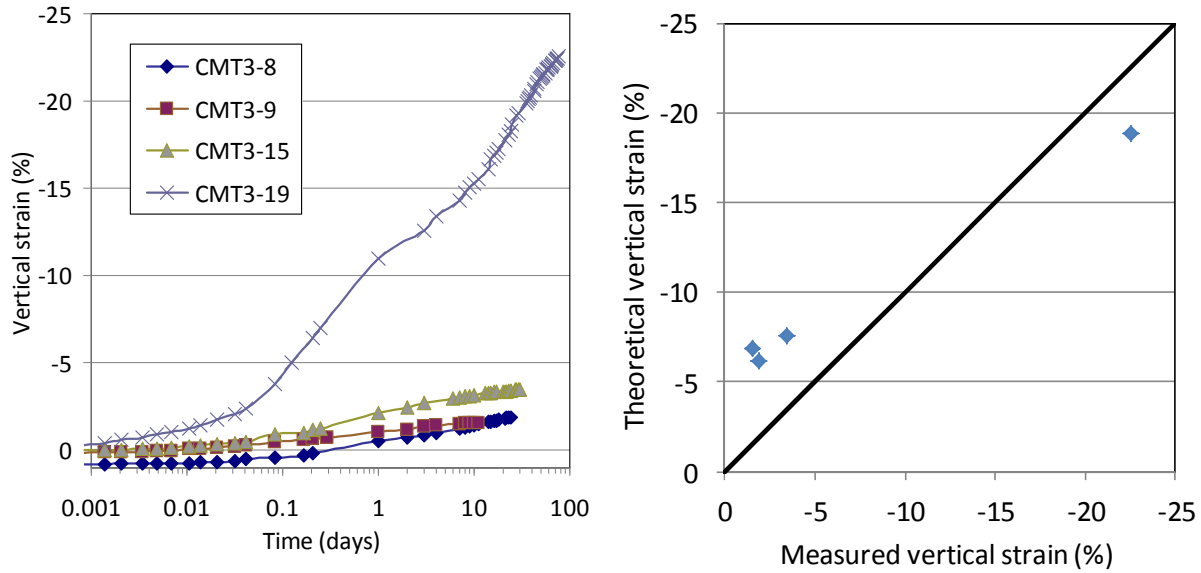

Figure 33: Evolution of vertical strain during the swelling under load tests performed with samples of the GBM (B-S samples, details in Table IV) and comparison of the final values with the theoretical ones obtained with Equation 3

In the same standard oedometers the swelling pressure of a sample saturated with deionised water was checked (sample B-S-CMT3-019). The swelling pressure of the GBM was also tested in some samples using Pearson water as saturating solution in the high pressure oedometers prior to the determination of hydraulic conductivity (Table III). The results are detailed in Table V and plotted in Figure 34. The swelling pressure was found to be slightly below the theoretical values for untreated FEBEX bentonite tested with deionised water (Eq. 2), which was to be expected, since the swelling pressure decreases with the salinity of the solution, especially for low bentonite densities (Castellanos et al. 2008).

Table V: Summary of the swelling pressure tests performed in B-S samples

Reference	Water type	Initial ρ_d (g/cm^3)	Initial w (%)	Initial S_r (%)	P_s (MPa)	Duration (days)	Final w (%)	Final ρ_d (g/cm^3)	Final S_r (%)
CMT3-019	Deionised	36.3	1.34	97	0.69	7	43.2	1.33	113
CMT1-008[a]	Pearson	35.4	1.35	96	0.37	22	40.4[b]	1.35[c]	109
CMT3-024[a]	Pearson	40.9	1.18	85	0.33	17	45.7[c]	1.21[c]	101
B2-005[a]	Pearson	40.9	1.27	98	0.52	12	46.8[c]	1.26[c]	110

[a] performed in the high-pressure oedometer; [b] checked at the end of the permeability test; [c] computed at the end of the hydration phase from sensors' measurements

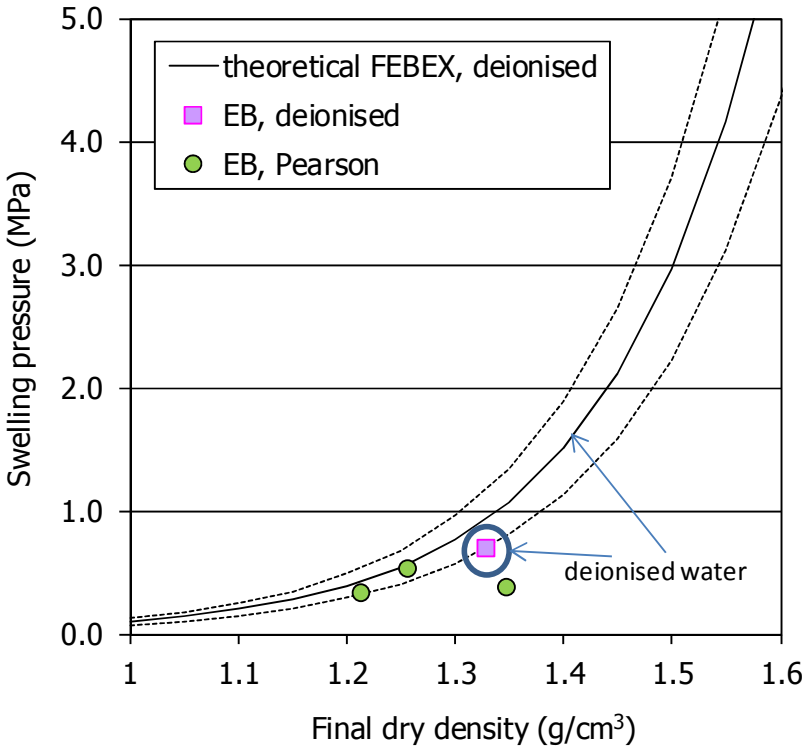

Figure 34: Swelling pressure determined in samples of GBM and empirical correlation for untreated FEBEX bentonite (Eq. 2)

6 Summary and conclusions

This report summarises the physical and thermo-hydro-mechanical characterisation performed at CIEMAT laboratories of bentonite samples taken during the EB experiment dismantling.

The water contents of the samples ranged between 33 and 43% and the dry densities between 1.42 and 1.24 g/cm^3, with a clear trend for the water content to increase towards the bottom part of the barrier (Villar 2013). Two factors could have played a role in this distribution. Firstly, during the installation of the GBM segregation occurred, the finer grains accumulating at the bottom, which would cause an initial density gradient in the barrier, with lower density at the bottom. Secondly, the effect of gravity on the water distribution seems to have been relevant. The accumulation of water in the lower part of the barrier took place probably at the beginning of the experiment, favoured by the higher initial porosity of the barrier bottom. The higher water contents in these zones were accompanied by a further reduction in dry densities,

consequence of swelling. This swelling seems to have been irreversible, since the density difference among different parts of the barrier remained after 10 years of operation. The blocks had water contents similar to those of the adjacent GBM, and their density decreased from an initial value of 1.7 g/cm^3 to values close to 1.4 g/cm^3, similar to the average values found in the GBM. The increase in the dimensions of the blocks confirms that they swelled during the test and also after dismantling, when the pressures were released. The blocks closer to the concrete plug swelled mainly in the longitudinal direction, whereas in the rest of sections the change in blocks' vertical dimensions indicates the uplift of the canister. Concerning the average values of water content and dry density there are not important differences among the different sampling sections.

The degrees of saturation of the barrier ranged between 95 and 101%. It is considered that the average pore water density in the barrier is close to 1.0 g/cm^3 due to the low average dry density of the bentonite.

The suction of the samples was computed from the relative humidity and temperature measured with psychrometers in the laboratory in samples of the blocks and the GBM. The values obtained ranged between 2.1 and 4.7 MPa. The suction decreased with water content, and no difference could be found between the GBM and the blocks. The suctions measured in the samples retrieved were higher than the values expected for untreated FEBEX samples of the same dry density and water content. The reason could be that the samples from the EB were saturated with saline water and would consequently have a high osmotic suction.

The pore size distribution determined by MIP showed that during operation the GBM developed a macropore family with diameters between 3 and 35 µm that did not exist in the original material. However, most of the porosity of the samples analysed belonged to the microporosity size (diameter smaller than 7 nm), except for the samples of dry density lower than 1.3 g/cm^3, in which macroporosity was predominant. The basal spacings of the smectite indicate that in most samples 3 water layers were completely developed in the interlayer. For water contents approximately below 38% the basal spacing increased with the water content, but for higher values the basal spacings did not seem to depend on the water content and were similar to values of FEBEX bentonite samples of the same water content saturated with deionised water.

The superficial thermal conductivity was between 0.95 and 1.33 W/m·K, with a trend to find higher values in the GBM than in the blocks for samples of the same water content. These values are below those measured in blocks of untreated FEBEX bentonite compacted at degrees of saturation close to 100%, which were above 1.2 W/m·K. The relation of thermal conductivity with dry density and water content was not clear, probably because all the samples were virtually saturated. Nevertheless it seemed that the dry density had a higher contribution to thermal conductivity than the water content.

The hydraulic conductivities measured in the GBM samples retrieved were in the range from $8 \cdot 10^{-12}$ to $2 \cdot 10^{-13}$ m/s, mainly related to the dry density of the samples. These values were determined using Pearson water as fluid. When comparing these values to those expected for untreated FEBEX bentonite of the same dry density permeated with deionised water, it was found that the values for the GBM were slightly above the theoretical ones, but mostly inside the expected range of variation. This can be attributed to the different salinity of the water used in the tests, since a higher salinity would increase permeability. Consequently, it is considered that the permeability of the GBM did not change during operation.

The swelling pressure of the GBM was also tested in some samples using Pearson water as saturating solution. It was found to be slightly below the values expected for untreated FEBEX bentonite tested with deionised water, which was to be expected, since the swelling pressure

decreases with the salinity of the solution, especially for low bentonite densities. However, when tested with deionised water, the swelling capacity seemed to recover once chemical equilibrium was reached.

Acknowledgements

The research leading to these results received funding from the European Atomic Energy Community's Seventh Framework Programme (FP7/2007-2011) under Grant Agreement n°249681, the PEBS project. This work was additionally financed by ENRESA through a CIEMAT-ENRESA General Agreement. The laboratory work was performed by Juan Aroz, Francisco Javier Romero, Ana María González and Ramón Campos, at CIEMAT. The psychrometers used for suction measurement were lent by AITEMIN.

References

AITEMIN 2012. Engineered Barrier Emplacement Experiment in Opalinus Clay "EB" Experiment. TEST PLAN. Madrid, 64 pp.

CASTELLANOS, E., VILLAR, M.V., ROMERO, E., LLORET, A. & GENS, A. 2008. Chemical impact on the hydro-mechanical behaviour of high-density FEBEX bentonite. *Physics and Chemistry of the Earth* 33: S516-S526.

ENRESA 2005. "Engineered barrier emplacement experiment in Opalinus Clay for the disposal of radioactive waste in underground repositories" Final Report. *Publicación Técnica ENRESA* 02/05. Madrid, 101 pp.

ENRESA, 2006. FEBEX Full-scale Engineered Barriers Experiment, Updated Final Report 1994-2004. *Publicación Técnica ENRESA* 05-0/2006, Madrid, 590 pp.

IMBERT, CH. & VILLAR, M.V. 2006. Hydro-mechanical response of a bentonite pellets/powder mixture upon infiltration. *Applied Clay Science* 32: 197-209.

KYOTO ELECTRONICS MANUFACTURING CO. 1987. Kemtherm QTM-D3 Quick Thermal Conductivity Meter Instruction Manual. Tokyo, 19 pp.

SING, K.S.W., EVERETT, D.H., HAUL, R.A.W., MOSCOU, L., PIEROTTI, R.A., ROUQUÉROL, J., SIEMIENIEWSKA, T. 1985. Reporting physisorption data for gas/solid systems with special reference to the determination of surface area and porosity. *Pure & Appl. Chem*. 57(4): 603-619. IUPAC.

PEARSON F. 1998. Artificial waters for use in laboratory and field experiments with Opalinus Clay. *Paul Scherrer Institut TM* 44-98-08

UNE 7045(1952): Determinación de la porosidad de un terreno.

GUTIÉRREZ-NEBOT, L. 2013. Informe de caracterización de fases sólidas mediante XRD. CIEMAT, Residuos Radiactivos, Referencia 0306 0219 0122. Madrid, 90 pp.

PALACIOS, B., REY M. & GARCÍA-SIÑERIZ, J.L. 2013. Engineered Barrier Emplacement Experiment in Opalinus Clay: "EB" Experiment. As-built of dismantling operation. PEBS Deliverable-n°: D2.1-4. Contract Grant Agreement Number FP7 249681. AITEMIN, 95 pp.

VILLAR, M.V. 2002. Thermo-hydro-mechanical characterisation of a bentonite from Cabo de Gata. A study applied to the use of bentonite as sealing material in high level radioactive waste repositories. *Publicación Técnica ENRESA* 01/2002. Madrid, 258 pp.

VILLAR, M.V. 2012. EB experiment. Laboratory infiltration tests report. PEBS Deliverable 2.1-5. *Technical Report* CIEMAT/DMA/2G210/07/12. Madrid, 33 pp.

VILLAR, M.V. 2013. EB Experiment. Contribution of CIEMAT to EB dismantling report. Physical state of the bentonite. EC Contract 249681 PEBS. *Informe Técnico* CIEMAT/DMA/2G210/04/2013. Madrid, 21 pp.

VILLAR, M.V. & LLORET, A. 2008. Influence of dry density and water content on the swelling of a compacted bentonite. *Applied Clay Science* 39: 38-49.

VILLAR, M.V., GÓMEZ-ESPINA, R. & GUTIÉRREZ-NEBOT, L. 2012a. Basal spacings of compacted bentonite. *Applied Clay Science* 65-66: 95-105.

VILLAR, M.V., MARTÍN, P.L., BÁRCENA, I., GARCÍA-SIÑERIZ, J.L., GÓMEZ-ESPINA R. & LLORET A. 2012b. Long-term experimental evidences of saturation of compacted bentonite under repository conditions. *Engineering Geology* 149-150: 57-69.

Appendix 1 Physical measurements

Table A1 I: Values measured in the laboratory in GBM samples from section A1_25 (z=320)

Sample reference	x	y	Dry density (g/cm^3)	Water content (%)	Degree of saturation (%)
B-S-A1_25-018	49	107	1.30	41.0	102
B-S-A1_25-019	57	100	1.35	36.5	98
B-S-A1_25-020	67	90	1.38	35.5	100
B-S-A1_25-021	83	80	1.35	35.9	97
B-S-A1_25-022	100	70	1.34	37.0	99
B-S-A1_25-023	125	60	1.34	36.7	97
B-S-A1_25-024	140	50	1.31	38.0	97
Average			1.34±0.03	37.2±1.9	99±2

Table A1 II: Values measured in the laboratory in block samples (two or three measurements per sample for dry density and water content, average specimen volume 10±2 cm^3; average of 3 measurements for thermal conductivity, λ) from section CMT1 (z=355)

Sample reference	Position[a] (cm)	Dry density (g/cm^3)	Water content (%)	Degree of saturation (%)	Suction (MPa)	*d*(001) (nm)	λ (W/m·K)
B-B-CMT1-007	53	1.39	33.9	98	4.7[c]	1.284	1.07
	62	1.39	34.0	97		1.318	
	70	1.39	34.8	99		1.699	
B-B-CMT1-006	79	1.37	34.4	96			1.19[e]
	88	1.37	34.4	95			1.19[e]
	96	1.35	35.3	95			
B-B-CMT1-004	105	1.33	38.8	102		2.149	1.05[e]
	114	1.34	37.0	98	0[b]	1.654	
	123	1.35	35.9	97	0.5[b]	2.029[d]	1.18[f]
Average		1.36±0.02	35.4±1.6	97±2			

[a]Approximate distance to canister axis; [b]Measured in the laboratory with capacitive sensors; [c]Measured in the laboratory with psychrometers; [d]Double peak; [e]Parallel to compaction; [f]Perpendicular to compaction

Table A1 III: Values measured in the laboratory in block samples (two or three measurements per sample for dry density and water content, average specimen volume 11±2 cm^3; average of 3 measurements for thermal conductivity, λ, and 2 measurements for solid grain density, γ) from section CMT2 (z=460)

Sample reference	Position[a] (cm)	Dry density (g/cm^3)	Water content (%)	Degree of saturation (%)	Suction[b] (MPa)	*d*(001) (nm)	λ (W/m·K)	γ (g/cm^3)
B-B-CMT2-002	53	1.39	33.3	96		2.085[c]	1.19[d]	
	62	1.39	32.9	94		1.732		
	70	1.40	33.6	98	4.5	1.826		
B-B-CMT2-005	79	1.39	35.2	100		1.843		2.70
	88	1.38	34.8	98		1.581	1.15[d]	2.72
	96	1.38	35.3	99	3.6	1.707[c]		2.69
B-B-CMT2-009	105	1.37	35.9	99		2.096[c]		2.66
	114	1.38	35.7	101				2.72
	123	1.37	35.6	98	3.2	1.970		2.72
Average		1.38±0.01	34.7±1.1	98±2				

[a]Approximate distance to canister axis; [b]Measured in the laboratory with capacitive sensors; [c]Double peak; [d]Parallel to compaction

Table A1 IV: Values measured in the laboratory in block samples (two or three measurements per sample for dry density and water content, average specimen volume 10±1 cm^3; average of 3 measurements for thermal conductivity, λ) from section CMT3 (z=650)

Sample reference	Position[a] (cm)	Dry density (g/cm^3)	Water content (%)	Degree of saturation (%)	Suction[b] (MPa)	λ[d] (W/m·K)
B-B-CMT3-001	53	1.38	35.0	99		0.95
	62	1.35	35.6	96		
	70	1.36	36.0	99	2.9	
B-B-CMT3-003	79	1.34	36.3	97	2.7	1.09
	88	1.36	35.6	97		
	96	1.37	35.8	100		1.07
B-B-CMT3-006	105	1.37	35.3	98		1.16
	114	1.37	34.8	97	2.3	
	123	1.36	35.2	97		1.08
Average		1.36±0.01	35.5±0.5	98±1		

[a]Approximate distance to canister axis; [b]Measured in the laboratory with capacitive sensors; [c]Measured in the laboratory with psychrometers; [d]Parallel to compaction

Table A1 V: Values measured in the laboratory in GBM samples (two measurements per sample for dry density and water content, average specimen volume 12±3 cm^3) from section CMT1 (z=349)

Sample reference	x	y	Dry density (g/cm^3)	Water content (%)	Degree of saturation (%)	Suction (MPa)	*d*(001) (nm)
B-S-CMT1-001	-58	105	1.35	37.3	100		
B-S-CMT1-002	-78	95	1.35	36.0	97		
B-S-CMT1-003	-105	81	1.33	37.0	97		2.142[c]
B-S-CMT1-004	-130	68	1.30	39.8	100	2.0[a]	2.186[c]
B-S-CMT1-005	65	112	1.36	35.6	97		1.818
B-S-CMT1-006	84	113	1.36	36.3	99	1.2[a] / 4.3[b]	1.829
B-S-CMT1-007	111	114	1.36	35.3	97	4.3[b]	
B-S-CMT1-008	132	114	1.36	36.3	99	3.1[b]	2.195[c]
B-S-CMT1-017	0	182	1.41	34.1	100	4.0[b]	2.290[c]
B-S-CMT1-018	0	195	1.42	32.8	98	3.4[b]	1.806
B-S-CMT1-016	0	235	1.43	32.3	98		1.763
B-S-CMT1-019	0	250	1.40	34.3	100	2.2[a] / 4.6[b]	1.785
Average			1.37±0.04	35.6±2.0	99±1		

[a]Measured in the laboratory with capacitive sensors; [b]Measured in the laboratory with psychrometers; [c]Double peak

Table A1 VI: Values measured in the laboratory in GBM samples (two measurements per sample for dry density and water content, average specimen volume 8±1 cm^3) from section CMT2 (z=460)

Sample reference	x	y	Dry density (g/cm^3)	Water content (%)	Degree of saturation (%)	Suction[a] (MPa)	*d*(001) (nm)
B-S-CMT2-004	55	127	1.33	37.2	97		1.601
B-S-CMT2-005	81	127	1.33	37.4	98		1.926
B-S-CMT2-006	107	127	1.37	35.1	98	3.0	
B-S-CMT2-007	134	127	1.35	36.2	97		1.800
B-S-CMT2-018	-53	110	1.34	37.7	100		1.752[b]
B-S-CMT2-019	-81	123	1.30	38.3	97		1.703[b]
B-S-CMT2-020	-111	103	1.29	39.2	97		
B-S-CMT2-021	-120	95	1.18	46.2	97	3.4	
B-S-CMT2-026	95	189	1.38	35.5	100		1.959[b]
B-S-CMT2-029	0	187	1.42	32.0	96		
B-S-CMT2-030	0	207	1.39	33.3	96		1.652
B-S-CMT2-031	0	227	1.42	32.8	98		1.736
B-S-CMT2-032	0	250	1.42	33.5	100		1.880[b]
Average			1.35±0.07	36.4±3.7	98±1		
B-S-CMT2-015	-96	93	1.30	39.0	97		
B-S-CMT2-017	-129	31	1.17	48.3	99		2.082[b]

[a]Measured in the laboratory with psychrometers; [b]Double peak

Table A1 VII: Values measured in the laboratory in GBM samples (two measurements per sample for dry density and water content, average specimen volume 9±1 cm^3; average of 3 measurements for thermal conductivity, λ) from section CMT3 (z=695)

Sample reference	x	y	Dry density (g/cm^3)	Water content (%)	Degree of saturation (%)	Suction[a] (MPa)	*d*(001) (nm)	λ (W/m·K)
B-S-CMT3-008	65	127	1.35	35.6	96		1.706[d]	
B-S-CMT3-009	90	127	1.34	36.0	96		1.923[d]	1.17
B-S-CMT3-010	110	127	1.35	36.0	97		1.834	0.97
B-S-CMT3-011	125	127	1.34	35.6	95		1.906	1.07
B-S-CMT3-014	65	200	1.38	34.6	98		1.827	1.35
B-S-CMT3-015	0	180	1.38	35.7	100	3.7	1.655	1.35
B-S-CMT3-016	0	195	1.39	34.6	99	4.5	1.731[d]	0.39
B-S-CMT3-017	0	215	1.39	34.7	99		1.827[d]	1.19
B-S-CMT3-018	0	235	1.39	35.3	101	4.0	2.206	1.23
B-S-CMT3-019	-55	127	1.31	38.7	99		1.911[d]	1.33
B-S-CMT3-020	-60	127	1.32	38.0	98		1.893	1.15
B-S-CMT3-021	-82	127	1.29	39.6	97	2.6	1.735	
B-S-CMT3-022	-124	127	1.23	43.8	100		1.827[d]	
Average[b]			1.34±0.05	36.8±2.6	98±2			
B-S-CMT3-001	41	90	1.30	41.3	103		1.998	
B-S-CMT3-002	94	55	1.27	43.1	103		1.953	
B-S-CMT3-003	129	30	1.17	47.8	99		1.914	
B-S-CMT3-023	-40	105	1.26	41.4	98			
B-S-CMT3-024	-95	70	1.27	40.9	99		1.985[d]	0.91
B-S-CMT3-025	-135	35	1.14	50.1	99		2.035[d]	1.02
Average[c]			1.31±0.07	39.3±4.6	99±2			

[a]Measured in the laboratory with psychrometers; [b]Samples from the 3 sampling radii in the half upper part of the GBM; [c]Samples from the 5 sampling radii; [d]Double peak

Table A1 VIII: Values measured in the laboratory in GBM samples (two measurements per sample for dry density and water content, average specimen volume 7±1 cm^3) from section E (z=520)

Sample reference	x	y	Dry density (g/cm^3)	Water content (%)	Degree of saturation (%)	Suction[a] (MPa)	*d*(001) (nm)
B-S-E-017	-67	128	1.37	34.9	97		
B-S-E-019	-112	127	1.37	34.2	95		
B-S-E-022	80	128	1.36	35.6	98		
B-S-E-023	94	127	1.36	36.0	99		
B-S-E-024	132	128	1.38	35.4	100		1.784
B-S-E-028	68	161	1.37	35.5	99		

Sample reference	x	y	Dry density (g/cm^3)	Water content (%)	Degree of saturation (%)	Suction[a] (MPa)	*d*(001) (nm)
B-S-E-029	96	178	1.41	33.8	99		
B-S-E-032	-57	170	1.38	34.2	97		
B-S-E-034	-80	195	1.40	33.9	99		
B-S-E-037	0	180	1.39	34.3	98		
B-S-E-038	0	203	1.39	33.8	98		
B-S-E-039	0	219	1.42	33.1	98	4.7	1.821
B-S-E-040	0	240	1.36	35.3	97		
Average[b]			1.38±0.02	34.6±0.9	98±1		
B-S-E-010	-57	107	1.36	35.4	97		
B-S-E-012	-87	81	1.36	35.5	98		
B-S-E-014	-106	63	1.24	42.5	98		
B-S-E-016	-133	25	1.13	51.7	101	2.1	2.097[d]
Average[c]			1.36±0.07	36.2±4.5	98±1		

[a]Measured in the laboratory with psychrometers; [b]Samples from the half upper part of the GBM; [c]Samples from all the sampling radii; [d]Double peak

Table A1 IX: Values measured in the laboratory in GBM samples (two measurements per sample for dry density and water content, average specimen volume 8±2 cm^3) from section B2 (z=647)

Sample reference	x	y	Dry density (g/cm^3)	Water content (%)	Degree of saturation (%)	Suction (MPa)	*d*(001) (nm)
B-S-B2-031	-35	168	1.37	35.0	97		
B-S-B2-032	-45	176	1.36	35.2	97	2.0[a]	
B-S-B2-033	-55	186	1.37	35.3	98		
B-S-B2-034	-65	199	1.37	35.0	97	1.2[a]	
B-S-B2-035	-75	214	1.37	35.2	98		
Average[c]			1.37±0.00	35.2±0.2	97±1		
B-S-B2-001	48	101	1.29	39.6	98		
B-S-B2-002	58	95	1.30	38.7	97		
B-S-B2-003	67	85	1.31	38.8	99		
B-S-B2-004	82	75	1.29	40.2	99		
B-S-B2-005	102	62	1.29	39.6	98		
B-S-B2-006	119	50	1.21	44.5	97		
B-S-B2-007	129	40	1.19	45.6	96	2.3[b]	1.984[e]
B-S-B2-020	-124	29	1.12	50.3	96	2.9[b]	2.132[e]
Average[d]			1.25±0.07	42.2±4.2	97±1		

[a]Measured in the laboratory with capacitive sensors; [b]Measured in the laboratory with psychrometers; [c]Samples from the half upper part of the GBM; [d]Samples from the half lower part of the GBM; [e]Double peak

Appendix 2 Pore size distribution measurements

Table A2 I: Mercury intrusion porosimetry results for EB samples of sampling section B2

Reference[a]	Time[b] (days)	ρ_d (g/cm^3)	*w* (%)	% intruded	% macro	% meso	% micro	Mode macro (nm)	Mode meso (nm)
BS-B2-007	23	1.19	45.6	55	49	6	45	12369	7
BS-B2-020	22	1.12	50.3	60	54	6	40	20859	9

[a] B-S: GBM sample; [b] time elapsed from sampling to lyophilisation

Table A2 II: Mercury intrusion porosimetry results for EB samples of sampling section CMT1

Reference[a]	Time[b] (days)	ρ_d (g/cm^3)	*w* (%)	% intruded	% macro	% meso	% micro	Mode macro (nm)	Mode meso (nm)
B-S-CMT1-003	35	1.33	37.0	45	36	9	55	11126	9
B-S-CMT1-004	39	1.30	39.8	51	41	10	49	11124	7
B-S-CMT1-005	36	1.36	35.6	52	41	15	43	12346	14
B-S-CMT1-006	39	1.36	36.3	48	39	17	44	12348	11
B-S-CMT1-007	41	1.36	35.3	50	41	10	50	18791	17
B-S-CMT1-008	39	1.36	36.3	53	43	10	47	18796	8
B-S-CMT1-016	41	1.43	32.3	46	35	10	54	11124	12
B-S-CMT1-017	41	1.41	34.1	46	36	12	52	9027	11
BS-CMT1-018	41	1.42	32.8	51	39	15	46	12375	11
BS-CMT1-019	39	1.40	34.3	50	39	11	50	13741	11
BB-CMT1-004a	38	1.35	35.9	55	44	12	45	5352	12
BB-CMT1-004m	38	1.34	37.0	47	34	13	53	2997	10
BB-CMT1-004h	38	1.33	38.8	49	37	12	51	3745	10
BB-CMT1-007a	59	1.39	34.8	52	38	13	48	2981	11
BB-CMT1-007m	59	1.39	34.0	47	34	20	45	4823	10
BB-CMT1-007h	59	1.39	33.9	50	37	13	50	3753	11

[a] B-S: GBM sample, BB: block, a: top of block, m: middle part of block, h: bottom of block (in relation to the position of the block in the barrier); [b] time elapsed from sampling to lyophilisation

Table A2 III: Mercury intrusion porosimetry results for EB samples of sampling section CMT2

Reference[a]	Time[b] (days)	ρ_d (g/cm^3)	*w* (%)	% intruded	% macro	% meso	% micro	Mode macro (nm)	Mode meso (nm)
BS-CMT2-004	11	1.33	37.2	55	46	9	45	18794	9
BS-CMT2-005	12	1.33	37.4	55	46	9	45	12345	14
BS-CMT2-007	12	1.35	36.2	50	41	9	50	20866	23
BS-CMT2-017	89	1.17	48.3	64	57	7	36	35180	11
BS-CMT2-018	12	1.34	37.7	48	40	7	52	3352	19
BS-CMT2-019	12	1.30	38.3	55	46	8	45	15256	15
BS-CMT2-020	11	1.29	39.2	50	42	7	50	3348	9
BS-CMT2-021	11	1.18	46.2	58	52	6	42	2684	10
BS-CMT2-026	75	1.38	35.5	54	45	9	46	12346	8
BS-CMT2-030	12	1.39	33.3	45	36	9	55	2686	10
BS-CMT2-031	11	1.42	32.8	49	39	10	51	2671	17
BS-CMT2-032	12	1.42	33.5	48	39	9	52	3353	14
BB-CMT2-002a	35	1.39	33.3	53	39	13	47	18792	10
BB-CMT2-002m	35	1.39	32.9	50	36	14	50	18793	9
BB-CMT2-002h	35	1.40	33.6	53	39	14	47	23151	10
BB-CMT2-005a	33	1.39	35.2	50	38	12	50	15251	7
BB-CMT2-005m	33	1.38	34.8	53	41	12	47	18786	15
BB-CMT2-005h	33	1.38	35.3	51	38	13	49	18779	17
BB-CMT2-009a	34	1.37	35.9	51	38	13	49	15250	10
BB-CMT2-009m	34	1.37	35.6	52	39	13	48	16920	11
BB-CMT2-009h	34	1.38	35.7	54	40	14	46	15249	12

[a] B-S: GBM sample, BB: block, a: top of block, m: middle part of block, h: bottom of block (in relation to the position of the block in the barrier); [b] time elapsed from sampling to lyophilisation

Table A2 IV: Mercury intrusion porosimetry results for EB samples of sampling section CMT3

Reference[a]	Time[b] (days)	ρ_d (g/cm^3)	*w* (%)	% intruded	% macro	% meso	% micro	Mode macro (nm)	Mode meso (nm)
BS-CMT3-001	70	1.30	41.3	56	47	9	44	12342	12
BS-CMT3-002	57	1.27	43.1	50	41	9	50	15258	14
BS-CMT3-003	52	1.17	47.8	54	46	7	46	16923	7
BS-CMT3-023	56	1.26	41.4	53	45	8	47	8136	14
BS-CMT3-024	34	1.27	40.9	75	68	8	25	11125	7
BS-CMT3-025	52	1.14	50.1	57	50	7	43	35166	11

[a] B-S: GBM sample; [b] time elapsed from sampling to lyophylisation